

Interfacial dynamics and structure of surfactant layers

Boris Zhmud^{a,*}, Fredrik Tiberg^b

^a*Institute for Surface Chemistry, Box 5607, SE-114 86 Stockholm, Sweden*

^b*Camurus AB, Ideon Science Park, Sölvegatan 41, SE-223 70 Lund, Sweden and Physical Chemistry 1, Box 124 Lund University, SE-22100 Lund, Sweden*

Abstract

The present article provides current opinion on studies of the interfacial dynamics, adsorption, and structure of surfactant layers. The physical principles and applications of physicochemical methods such as tensiometry, ellipsometry, photon correlation spectroscopy, and neutron reflectivity techniques, as well as relevant theoretical aspects related to the adsorption and desorption kinetics, interfacial structure development, wetting enhancement, and the effect of adsorbed surfactant films of the interfacial dynamics, are covered in detail. In order to make the text as self-contained as possible, essential mathematical derivations are given demonstrating how raw data, such as ellipsometric angles or neutron reflectivity, are transformed into sought layer characteristics, such as thickness or density.

© 2005 Elsevier B.V. All rights reserved.

Contents

1. Introduction	22
2. Experimental methods for studying the properties of surfactants at interfaces	22
2.1. Adsorption of surfactants	22
2.1.1. Surface tensiometry	22
2.2. Structure and composition of adsorbed surfactant layers	24
2.2.1. Ellipsometry	24
2.2.2. Photon correlation spectroscopy	26
2.2.3. Small-angle neutron scattering	27
2.2.4. Neutron reflectivity	29
3. Dynamics of surfactant adsorption and surface tension relaxation	30
3.1. Diffusion-controlled adsorption kinetics	30
3.2. Activation-controlled adsorption kinetics	32
3.3. Mixed adsorption kinetics	32
3.4. Adsorption from micellar solutions	32
3.5. Adsorption of mixed surfactants	33
4. Intermolecular interactions in aggregated surfactant	34
5. A review of experimental studies on the dynamics and structure of surfactant layers	35
6. Wetting enhancement by surfactants	37
6.1. Thermodynamic consideration	37
6.2. Dynamics of surfactant-induced drop spreading	38

* Corresponding author.

E-mail address: boris.zhmud@sveacon.se (B. Zhmud).

7. Effect of surfactants on the damping of capillary waves	39
8. Concluding remarks	41
References	41

1. Introduction

Surfactants are ubiquitous in many technological and natural processes. Apart from traditional applications as detergents, emulsifiers and dispersing aids, and wetting and flotation agents, they have a tremendous and not yet fully appreciated potential for engineering functional interfaces and surface coatings. There exist many industrial processes involving free interfaces, for example, curtain coating and inkjet printing, whose performance is strongly influenced by surfactants. The word “process” refers to something dynamic rather than static, and hence, it is perhaps not so surprising that many actual processes – such as coalescence and break-up of emulsion droplets, liquid film levelling, foam growth and decay, surfactant-induced drop spreading, etc. – involving surfactants occur under nonequilibrium conditions, adding a time variable to the process description.

The relation between the chemical structure and the adsorption ability of surfactant molecules has been and remains one of the central issues in surfactant science. The adsorption behaviour of surfactants is traditionally characterized by measuring the surface tension of surfactant solutions over a range of surfactant concentrations. However, this gives no information about the structural arrangement of adsorbed molecules. A useful physical tool that can provide such information is reflection ellipsometry [1]. Surfactant self-aggregation in the bulk phase can be investigated with a variety of physicochemical methods including size exclusion chromatography, small-angle neutron scattering (SANS), electron spin resonance (ESR), nuclear magnetic resonance (NMR), photon correlation spectroscopy, fluorescence spectroscopy and cryo-transmission electron microscopy (cryo-TEM) [2–13]. In past decades, this arsenal has been supplemented by atomic force microscopy (AFM), neutron reflectivity and non-linear optical methods, opening up new vistas in the research on static and transient nano-structures formed by surfactants in solutions and at interfaces [14–16].

The present article was intended to cover the physical principles of some of those techniques, as well as certain theoretical aspects related to the adsorption and desorption kinetics, interfacial structure development, wetting enhancement and the effect of adsorbed surfactant films of the interfacial dynamics. In order to make the text as self-contained as possible, essential mathematical derivations are given demonstrating how raw data, such as ellipsometric angles or neutron reflectivity, are transformed into sought layer characteristics, such as thickness or density. Herewith, the mathematical rigor is sacrificed to physical clarity. It was not attempted – nor was it feasible – to touch on all the

experimental methods available. The main emphasis is put on those methods which are rather versatile and most often used in the authors’ own work.

2. Experimental methods for studying the properties of surfactants at interfaces

2.1. Adsorption of surfactants

2.1.1. Surface tensiometry

2.1.1.1. Thermodynamic background. The amount of surfactant adsorbed to the air/solution interface can be determined by measuring the surface tension, γ , of the solution. The common ground on which all the tensiometric methods are based is the Gibbs equation [17],

$$d\gamma + \sum_i \Gamma_i d\mu_i = 0 \quad (1)$$

where μ_i denotes the chemical potential, and Γ_i , the surface excess, of the i th surface-active component. For a diluted single-surfactant solution, μ , and so Γ , are functions of the bulk concentration, c , of surfactant. The situation becomes more complex when going to higher concentrations, especially in the case of multi-surfactant systems, where the chemical potential, μ_i , of each of the components is dependent on the concentrations of all the components present. As a consequence, the partial surface excess, Γ_i , of each of the surfactants in a multi-surfactant formulation will in general be a function of the bulk concentrations of all the surfactants present, i.e., $\Gamma_i = \Gamma_i(c_1, \dots, c_N)$. A common approach used for the description of multicomponent monolayers is the direct integration of the Gibbs equation using model adsorption isotherms. Although model isotherms may be chosen at will, it should be noted however that, in order to ensure thermodynamic consistency of the model, the partial adsorption isotherms, Γ_i and Γ_j , of the components i and j must satisfy the following constraint [18,19].

$$\frac{\partial}{\partial c_i} \left(\frac{\Gamma_j(c_1, c_2, \dots, c_N)}{c_j} \right) = \frac{\partial}{\partial c_j} \left(\frac{\Gamma_i(c_1, c_2, \dots, c_N)}{c_i} \right) \quad (2)$$

which directly follows from Eq. (1) after recalling that $d\mu_i = k_B T dc_i/c_i$, where k_B is the Boltzmann constant and T is the temperature. A comprehensive thermodynamic analysis of two-surfactant systems, including ionic/ionic, ionic/non-ionic, and nonionic/nonionic mixtures, has been conducted by Aratono et al. [20]. Also, theoretical models have been developed that take into account the possibility for reorgan-

ization and aggregation of surfactant molecules in adsorbed layers [21,22]. The effect of counterion binding on the surface tension of ionic surfactants has been considered by Kralchevsky et al. [23]. It is worth noting that the latter effect is an obvious consequence of the general thermodynamic result saying that adsorption of ions to an interface changes the interfacial free energy [24].

2.1.1.2. Static methods. The surface tension of a surfactant solution can be determined by a number of classical methods, such as the capillary rise method, the maximum bubble pressure method, the du Nouy ring method, and the pendant drop method. The details of those can be found in, e.g., Adamson's textbook [25]. The very brief outline and compilation of essential formulas are given below for reader's convenience.

(i) The capillary rise method consists in measuring the height, L , of capillary rise, of the solution in a cylindrical capillary of known radius, r ,

$$\gamma = \frac{r\rho gL}{2\cos\theta} \quad (3)$$

where ρ is the density of the solution, g is the acceleration of gravity, and θ is the contact angle. The capillary radius must be sufficiently small, $r \ll (\gamma/\rho g)^{1/2}$, for the above formula to be valid.

(ii) The maximum bubble pressure method consists in blowing air bubbles through a tiny tube projecting into the solution at a certain depth below the surface. Gas pressure in the bubble having the shape of a spherical cap goes through a maximum as its radius, $R(V)$, which is a function of the bubble volume, V , goes through a minimum ($dR/dV=0$ for the hemispherical shape). Experimentally, it suffices to measure the barrier gas pressure at which bubbles start to break away.

(iii) The du Nouy ring method consists in measuring the force, F , needed to detach a platinum ring from the surface of the solution. The surface tension is then found the simple force balance,

$$F = mg + 4\pi r\gamma \quad (4)$$

where m is the mass and r is the radius of the ring.

(iv) The Wilhelmy plate method is similar to the du Nouy ring method with the only exception that a thin plate is used instead of the ring.

(v) The pendant drop method consists in analysing the side profile of a drop hanging from a tip. Two drop dimensions: d_e , the equatorial diameter, and d_s , the diameter at the distance d_e up from the bottom of the drop are measured. The surface tension is then found as

$$\gamma = \frac{\rho g d_e^2}{H(S)}; \quad S = \frac{d_s}{d_e} \quad (5)$$

with the shape factor $H(S)$ determined for a broad range of d_s/d_e values.

There exist numerous embodiments of the abovementioned methods that improve their accuracy by applying a number of analytical or empirical corrections and by using

more sophisticated data acquisition and analysis procedures [26].

2.1.1.3. Dynamic methods. Since surfactant adsorption is a dynamic process, so is surface tension equilibration. Usually one talks about surface tension relaxation because the dynamic surface tension decreases from some initial value down to its equilibrium value (see, for example, Fig. 1).

A number of special dynamic techniques have been developed for the measurement of the surface tension dynamics with a time resolution of the order of 0.001 s. Of these the most popular are the oscillating jet method and the maximum bubble pressure method.

(i) *The maximum bubble pressure method.* The same technique as used in static surface tension determinations can be adapted for dynamic measurements by using different bubble formation rates. With increasing the bubble formation rate, the lifetime of each bubble, i.e., the time interval from the moment the bubble starts to grow up to the moment it reaches its hemispherical shape, decreases. In this way, time dependence of the surface tension can be deduced. The time range accessible to measurement is from 0.001 to 1 s.

Application of the dynamic maximum bubble pressure technique necessitates the determination of the pressure inside the bubble, the bubble formation frequency, and the effective surface age [27,28]. Approximately, the effective surface age can be taken equal one-half of the bubble lifetime. In a hypothetical case where the bubble formation rate is infinite, the effective surface age is zero. The surface tension of the zero-age surface is called (rather unfortunately) pure dynamic surface tension. It is important to note that the latter is in general different from the equilibrium surface tension of solvent and, in fact, there is no way to measure it experimentally.

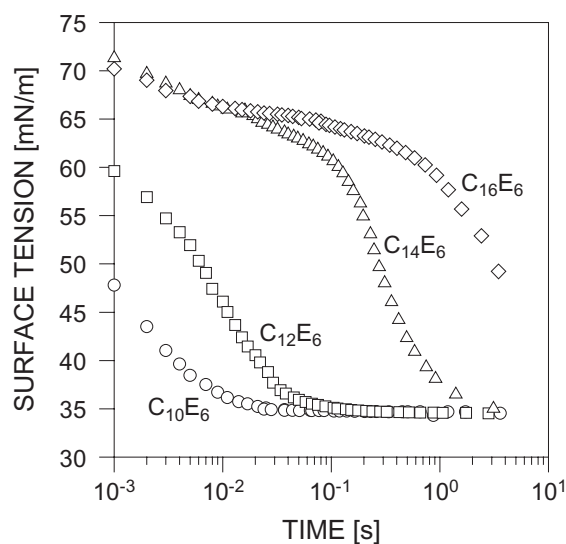


Fig. 1. Surface tension relaxation for 10 mM aqueous solutions of hexa(ethylene glycol) monoalkyl ethers $C_nH_{2n+1}(OCH_2CH_2)_6OH$ ($n=10,12,14,16$) with increasing aliphatic chain length.

(ii) *The oscillating jet method.* This method is best suited for studying solutions demonstrating high surface tension relaxation rates; the accessible time range is from 0.0001 to 0.1 s. The method is based on the fact that a liquid jet emerging from an elliptic orifice oscillates around the jet symmetry axis, tending to adopt a cylindrical shape. As a result, the jet looks wavy when is seen from a side. Let λ be the observed wavelength, Q , the volumetric flow rate, and r , the average jet radius. Then, in the first approximation, the surface tension can be calculated as,

$$\gamma = \frac{4\rho Q^2}{6r\lambda^2} \quad (6)$$

assuming the liquid inviscid and the amplitude of oscillations infinitesimal. A rigorous derivation of Eq. (6) can be found in [29]. However, it can also be obtained in a much simpler way using the dimensional analysis. Really, by taking into account that the frequency, ν , of jet oscillations scales as $\nu \propto (\gamma/\rho r^3)^{1/2}$, the velocity, v , of liquid scales as $v \propto Q/r^2$, and $\lambda = v/\nu$, one gets $\gamma \propto \rho Q^2/r\lambda^2$. In practice, correcting factors need to be introduced in the above equation in order to achieve a meaningful accuracy level. Thus, with corrections for viscosity and for a finite amplitude of oscillations, Eq. (6) reads [29]

$$\gamma = \frac{4\rho Q^2}{6r\lambda^2} \left[\frac{1 + 37/24(b^2/r^2)}{1 + 5/3(\pi^2 r^2/\lambda^2)} \right] \times \left[1 + 2 \left(\frac{\eta\lambda}{\rho Q} \right)^{3/2} + 3 \left(\frac{\eta\lambda}{\rho Q} \right)^2 \right] \quad (7)$$

where η is the viscosity of jetted solution, and b is the oscillation amplitude.

2.2. Structure and composition of adsorbed surfactant layers

2.2.1. Ellipsometry

Ellipsometry is a nondestructive optical technique for the determination of optical constants (thickness and refractive index) of thin films on surfaces. Transparent films from a tenth of angstrom up to several hundreds nanometers can be characterized. The physical principle on which ellipsometry rests is the fact that the polarization state of light changes when light is reflected from a surface. Monochromatic light represents an electromagnetic plane wave with the electric field vector, $\mathcal{E} = \mathbf{E} \exp[i(\omega t - \mathbf{k} \cdot \mathbf{r})]$, where ω is the circular frequency, and \mathbf{k} is the wave vector. Let a light beam illuminate a reflecting surface under oblique incidence. Then, the electric field vector can be resolved into two components, one lying in the plane of incidence and referred to as the p component, and the other one perpendicular to the plane of incidence and referred to as the s component. In general, these two components exhibit different reflective properties. Besides, when the light is reflected, the p and s components undergo different phase shifts. As a result, the ellipse of polarization changes upon reflection [30]. By measuring the change of polarization, it is possible to determine the ratio of

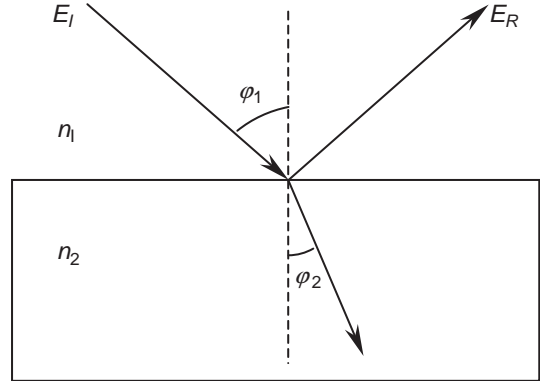


Fig. 2. Reflection and refraction of light at the boundary between two dielectrics with the refractive indices n_1 and n_2 . Here, φ_1 is the angle of incidence and φ_2 the angle of refraction.

the reflection coefficients, $r^{(p)}$ and $r^{(s)}$, which are in a simple way related to the refractive indices, n_1 and n_2 , of the bulk dielectric phases that form the light-reflecting interface,

$$r^{(p)} \equiv \frac{E_R^{(p)}}{E_I^{(p)}} = \frac{n_2 \cos \varphi_1 - n_1 \cos \varphi_2}{n_2 \cos \varphi_1 + n_1 \cos \varphi_2}$$

$$r^{(s)} \equiv \frac{E_R^{(s)}}{E_I^{(s)}} = \frac{n_1 \cos \varphi_1 - n_2 \cos \varphi_2}{n_1 \cos \varphi_1 + n_2 \cos \varphi_2} \quad (8)$$

where the superscripts I and R refer to the incident and reflected light beams, and the meaning of the angles φ_1 and φ_2 is clarified in Fig. 2. The above formulas can be easily derived from the boundary conditions for the electromagnetic field components.

Taking into account the law of refraction, $\sin \varphi_1 / \sin \varphi_2 = n_2 / n_1$, one can conclude that, in order to determine the Fresnel coefficients, it is sufficient to know the angle of incidence, φ_1 , and the refractive indices, n_1 and n_2 , of the contact phases.

In ellipsometry, it is customary to express the ratio, $r^{(p)}/r^{(s)}$, which in general is a complex number, via the so-called ellipsometric angles, Ψ and Δ , defined as [1]

$$\frac{r^{(p)}}{r^{(s)}} = \tan \Psi \exp[i\Delta]$$

$$\Psi = \arctan \left| \frac{r^{(p)}}{r^{(s)}} \right|; \quad \Delta = \zeta_p - \zeta_s \quad (9)$$

where ζ_p and ζ_s are the phases of the p and s components of the reflected light.

Now let a thin dielectric film (phase 2) be placed at the boundary between the phase 1 (ambient) and phase 3 (substrate) as shown in Fig. 3. The following expressions can be written for the incident (I), reflected (R), and transmitted (T) waves,

$$\begin{aligned} \text{Incident :} & \quad E_I \exp[i(\omega t - \mathbf{k}_1^+ \cdot \mathbf{r})] \\ \text{Reflected :} & \quad E_R \exp[i(\omega t - \mathbf{k}_1^- \cdot \mathbf{r})] \\ \text{Transmitted :} & \quad E_T \exp[i(\omega t - \mathbf{k}_3 \cdot \mathbf{r})] \end{aligned} \quad (10)$$

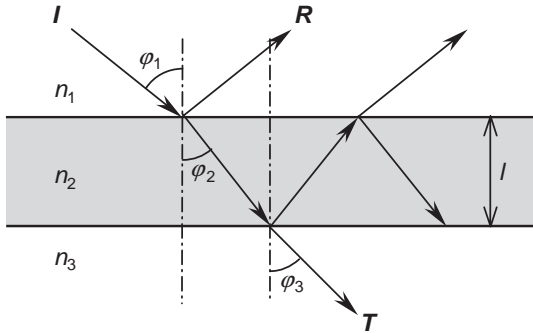


Fig. 3. Transmission of the electromagnetic wave through a uniform dielectric film separating two bulk dielectric phases.

In the film itself, there are two waves, $E_F^+ \exp[i(\omega t - \mathbf{k}_2^+ \cdot \mathbf{r})]$ and $E_F^- \exp[i(\omega t - \mathbf{k}_2^- \cdot \mathbf{r})]$ propagating, respectively, downwards and upwards (see Fig. 3). For each interface, two boundary conditions can be specified for the electromagnetic field components, giving four boundary conditions in total. This suffices for determining amplitude ratios for different waves. At the upper interface, one has

$$E_R = R_{12}E_I + D_{21}E_F^- = R_{12}E_I + \frac{1 - R_{12}^2}{D_{12}}E_F^-$$

$$E_F^+ = D_{12}E_I + R_{21}E_F^- = D_{12}E_I - R_{12}E_F^- \quad (11)$$

The physical meaning of these equations is quite transparent. For instance, the first of them simply states that the reflected wave is actually a superposition of two waves: one – described by the term $R_{12}E_I$ – reflected from the upper interface and the other one – described by the term $D_{21}E_F^-$ – reflected from the lower interface and refracted on the upper interface. Similar relations can be specified for the lower interface, with the only difference that the amplitudes E_F^+ and E_F^- must be corrected for the corresponding phase factors,

$$E_F^- \exp(ik_{2z}l) = R_{23}E_F^+ \exp(-ik_{2z}l)$$

$$E_T = D_{23}E_F^+ \exp(-ik_{2z}l) \quad (12)$$

where

$$k_{2z} = k_2 \cos \varphi_2 = \frac{2\pi}{\lambda} n_2 \cos \varphi_2$$

$$= \frac{2\pi}{\lambda} (n_2^2 - n_1^2 \sin^2 \varphi_1)^{1/2} \quad (13)$$

and the Fresnel coefficients R_{ij} and D_{ij} are defined as

$$R_{ij} = \frac{n_i \cos \varphi_i - n_j \cos \varphi_j}{n_i \cos \varphi_i + n_j \cos \varphi_j}$$

$$D_{ij} = \frac{2n_i \cos \varphi_i}{n_i \cos \varphi_i + n_j \cos \varphi_j} \quad (14)$$

By rearrangement of Eqs. (11) and (12), one gets

$$\frac{E_R}{E_I} = \frac{R_{12} + R_{23} \exp(-2ik_{2z}l)}{1 + R_{12}R_{23} \exp(-2ik_{2z}l)}$$

$$\frac{E_T}{E_I} = \frac{D_{12}D_{23} \exp(-ik_{2z}l)}{1 + R_{12}R_{23} \exp(-2ik_{2z}l)} \quad (15)$$

Recalling the definition of the ellipsometric ratio,

$$\tan \Psi \exp(i\Delta) \equiv \frac{E_R^{(p)}/E_I^{(p)}}{E_R^{(s)}/E_I^{(s)}} \quad (16)$$

and imposing a limitation by setting the polarization angle to 45° , in which case $E_I^{(s)} = E_I^{(p)}$, the main equation of ellipsometry is arrived at [1],

$$\tan \Psi \exp(i\Delta) = \frac{[R_{12}^{(p)} + R_{23}^{(p)} \exp(-i\beta)] [1 + R_{12}^{(s)} R_{23}^{(s)} \exp(-i\beta)]}{[R_{12}^{(s)} + R_{23}^{(s)} \exp(-i\beta)] [1 + R_{12}^{(p)} R_{23}^{(p)} \exp(-i\beta)]}$$

$$\beta = \frac{4\pi l}{\lambda} (n_2^2 - n_1^2 \sin^2 \varphi_1)^{1/2} \quad (17)$$

In the thin film limit, $l/\lambda \ll 1$, the exponents in Eq. (17) can be linearized, in which case $\text{Im}(E_R^{(p)}/E_R^{(s)}) \propto (l/\lambda) \times f(n_1, n_2, n_3)$, where $f(n_1, n_2, n_3)$ is some function of its arguments. Notice that the imaginary term, which contains information pertinent to the phase change of polarization caused by reflection, is linear in terms of l whereas the light intensity measured by classical reflectometry would scale as the square of l . This suggests that ellipsometry is best suited for thin film measurements; the practical accuracy level being around 1% of a monolayer.

In practice, the angles Ψ and Δ are determined from the orientations of the polarizer, compensator and analyzer. However, these angles are of little interest to the experimentalist, who wants to determine physical characteristics such as the refractive index, thickness or density of the adsorbed layer. To retrieve such information, an appropriate optical model linking the Ψ and Δ angles to the parameters of interest has to be used. In other words, ellipsometry is a model-dependent technique in a sense that the physical quantities of interest are not measured directly but only estimated in the framework of the model chosen. Different models may produce differing values of the quantities sought. It is also important to note that a single measurement affords only two real quantities characterizing the film. For instance, it is possible to determine the real refractive index and the thickness of the film, or the real and the imaginary parts of the complex refractive index provided that the film thickness is known. This limitation can be avoided by doing measurements at multiple angles of incidence or at different wavelengths. Ellipsometry can also be used to determine structural parameters of layered surfactant films by fitting an appro-

appropriate multilayer optical model to experimental data, though accuracy of such determinations is usually controversial.

After determining the thickness, l , and the refractive index, n , of the adsorbed film, it is possible to estimate the surface excess, $\Gamma(c)$, of adsorbate by expanding $n(c)$ into a power series and taking into account that the “concentration” of adsorbate in the film is $c=\Gamma(c)/l$,

$$\begin{aligned} n(c) &= n_0 + \sum_{k=1}^{\infty} \frac{c^k}{k!} \left. \frac{d^k n}{dc^k} \right|_{c=0} \\ &= n_0 + \sum_{k=1}^{\infty} \frac{(\Gamma/l)^k}{k!} \left. \frac{d^k n}{dc^k} \right|_{c=0} \end{aligned} \quad (18)$$

where n_0 is the refractive index of the ambient in the absence of adsorbate. Then $\Gamma(c)$ can be found, provided that n_0 and the derivatives $d^k n/dc^k$ are known or measured in an independent experiment (e.g., by refractometry). In most cases, only the linear term in the power-series expansion (18) is significant, so that

$$\Gamma(c) \frac{n(c) - n_0}{dn/dc} l \quad (19)$$

It should be noted that Eqs. (18) and (19) only apply to binary systems consisting of solvent and one adsorptive compound. For multi-component systems containing more than one adsorptive compound, the following generalization of Eq. (19) is possible,

$$\Delta_j n = \sum_{i=1}^N \frac{\Gamma_{ij}}{l_j} \left(\frac{\partial n}{\partial c_{ij}} \right)_{c_{ij}=0} \quad (20)$$

where $\Delta_j n \equiv n(c_{1j}, c_{2j}, \dots, c_{Nj}) - n_0$, $l_j \equiv l(c_{1j}, c_{2j}, \dots, c_{Nj})$ and $\Gamma_{ij} \equiv \Gamma_i(c_{1j}, c_{2j}, \dots, c_{Nj})$. This system of linear equations can be solved for Γ_{ij} provided that $\det [l_j^{-1} (\partial n / \partial c_{ij})_{c_{ij}=0}] \neq 0$ and the values of n , l and $\partial n / \partial c_{ij}$ have been determined for a sufficiently large number of differing adsorptive concentrations.

Ellipsometry is a powerful tool for tracking the time-evolution of adsorbed films (see Fig. 4). Other practical examples demonstrating the applications of ellipsometry for the study of adsorption/desorption dynamics of surfactants at various substrates can be found in numerous publications [31–36].

2.2.2. Photon correlation spectroscopy

When a monochromatic plane wave passes through a suspension of colloidal particles, it induces a dipole in each particle. The oscillating dipoles reemit electromagnetic waves of the same frequency as the incident wave but in different directions. This explains the mechanism of light scattering by colloids. The dipole induced in each particle is

$$\mathbf{p}_j = \alpha \mathbf{E}_0 \exp[i(\omega t - \mathbf{k} \cdot \mathbf{r}_j)] \quad (21)$$

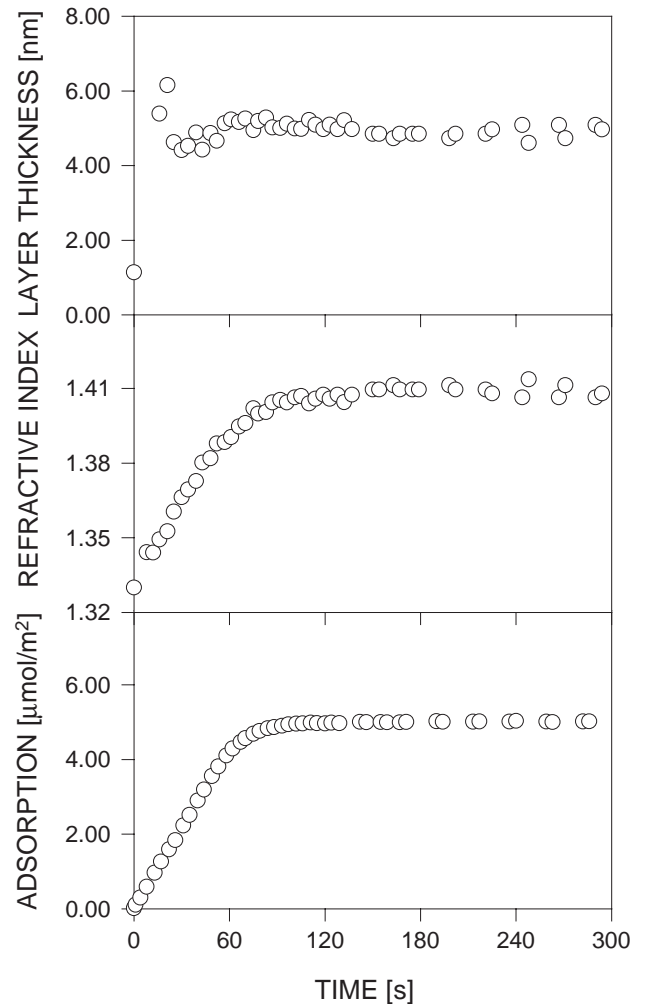


Fig. 4. Time dependence of surfactant layer thickness, refractive index, and surface excess measured by ellipsometry for 50 μM C_{14}E_6 surfactant adsorbed to the surface of silica (redrawn from Ref. [33]).

where

$$\alpha = \frac{n_p^2 (n_p^2 - n_0^2)}{n_p^2 + 2n_0^2} a^3 \quad (22)$$

in the case of spherical particles of radius a and refractive index n_p suspended in a medium with the refractive index n_0 . The magnitude of the electric field vector in the scattered light reaching the point \mathbf{R} where the detector is placed is found as the superposition of waves produced by individual dipoles,

$$E(\mathbf{R}, t) \propto \omega^2 \alpha E_0 \sum_j \frac{\exp[i(\omega t - \mathbf{k} \cdot \mathbf{r}_j - \varphi_j)]}{|\mathbf{R} - \mathbf{r}_j|} \quad (23)$$

where φ_j is the additional phase shift during the propagation of light to the detector. If the detector is placed sufficiently far from the sample, then $|\mathbf{R} - \mathbf{r}_j| \approx |\mathbf{R}|$ and

$\varphi_j \approx \mathbf{k}' \cdot (\mathbf{R} - \mathbf{r}_j)$ where \mathbf{k}' is the wave vector of the scattered wave. Consequently,

$$E(\mathbf{R}, t) \propto \frac{\omega^2 \alpha E_0}{|\mathbf{R}|} \exp[i(\omega t - \mathbf{k}' \cdot \mathbf{R})] \sum_j \exp[i\mathbf{q} \cdot \mathbf{r}_j] \quad (24)$$

where $\mathbf{q} = \mathbf{k}' - \mathbf{k}$ is the scattering vector.

In photon correlation spectroscopy, also known as dynamic light scattering, coherent light produced by a laser is used. The coherence of light preserves phase differences between the light scattered by different particles. If particles in the suspension were immobilized, a static diffraction pattern would be observed. However, the Brownian motion of particles causes the scattered light to fluctuate with time. To characterize these fluctuations, the field autocorrelation function is introduced [37],

$$\begin{aligned} f(t) &= E(\mathbf{R}, t)E^*(\mathbf{R}, 0) \propto \sum_{k,l} \exp[i\mathbf{q} \cdot (\mathbf{r}_k(t) - \mathbf{r}_l(0))] \\ &= \sum_k \exp[i\mathbf{q} \cdot (\mathbf{r}_k(t) - \mathbf{r}_k(0))] \\ &\quad + \sum_{k \neq l} \exp[i\mathbf{q} \cdot (\mathbf{r}_k(t) - \mathbf{r}_l(0))] \\ &= N \langle \exp[i\mathbf{q} \cdot (\mathbf{r}_1(t) - \mathbf{r}_1(0))] \rangle_N \\ &= N \left[1 + i\mathbf{q} \cdot \langle (\mathbf{r}_1(t) - \mathbf{r}_1(0)) \rangle_N \right. \\ &\quad \left. - \frac{1}{2} q^2 \langle (\mathbf{r}_1(t) - \mathbf{r}_1(0))^2 \rangle_N + \dots \right] \\ &= N [1 - q^2 D t + \dots] = N \exp(-q^2 D t) \end{aligned} \quad (25)$$

where the brackets $\langle \cdot \rangle_N$ mean averaging over the ensemble of particles and it is taken into account that $\langle (\mathbf{r}_1(t) - \mathbf{r}_1(0)) \rangle_N = 0$ and $\langle (\mathbf{r}_1(t) - \mathbf{r}_1(0))^2 \rangle_N = 2Dt$, where D is the diffusion coefficient of the particles and t is time. The field autocorrelation function exponentially decays with time; the characteristic decay time being

$$\tau = \frac{1}{q^2 D} = \frac{6\pi\eta a}{q^2 k_B T} \quad (26)$$

where η is the viscosity of the dispersing medium; the Stokes–Einstein equation has been used to link the diffusion coefficient to the size of the particles. It is the autocorrelation decay time that is measured experimentally, and then the size of scatterers is calculated using Eq. (26).

In practice, the intensity autocorrelation function,

$$Y(t) = \int_0^\infty I(\xi)I(t + \xi) d\xi \approx \sum_i I(\xi_i)I(t + \xi_i) \quad (27)$$

is used instead of $f(t)$. The intensity autocorrelation function is reconstructed by measuring a sequence of intensity values, $I(\xi_i)$ ($i=0,1,2,\dots$), on intervals of about 1 μs , from which the sequence of Y 's values is computed, $Y(\xi_j) = \sum_i I(\xi_i)I(\xi_j + \xi_i)$ ($j=1,2,\dots$). After reconstructing the intensity autocorrelation function, one can approximate it by the Siegert relation,

$$Y(t) = 1 + \exp(-2q^2 D t) \quad (28)$$

which permits the determination of the diffusion coefficient, D , and the hydrodynamic radius, $a = k_B T / 6\pi\eta D$, of dispersed particles. In the case of polydisperse systems, Eq. (28) is replaced by

$$Y(t) = 1 + \int_0^\infty A(a) \exp\left(-\frac{q^2 k_B T}{3\pi\eta a} t\right) da \quad (29)$$

from which the particle size distribution, $A(a)$, can be found.

Since the scattering intensity increases substantially when micelles are formed, photon correlation spectroscopy can be used for the study of aggregation phenomena in surfactant systems. By measuring the scattering intensities over the relevant range of surfactant concentrations, the cmc of the surfactant and the size of the micelles can be determined. Apart from routine applications in particle sizing, the method can also be used for studying the dynamic processes in surfactant-polymer systems, emulsions, microemulsions and colloids, and in particular, emulsification and dispersion processes aided by surfactants.

2.2.3. Small-angle neutron scattering

Neutron radiation can be produced over a broad range of energies, from over 10^5 eV (the de Broglie wavelength less than 10^{-14} m) in the case of fast neutrons to less than 10^{-7} eV (wavelength over 10^{-8} m) for ultracold neutrons. Two common sources of neutron radiation are nuclear reactors, where neutrons are generated by the fission of ^{235}U , and synchrotrons, where neutrons are produced by bombardment of heavy nuclei (e.g., Ta) with high-energy protons. In neutron scattering experiments, thermal and cold neutrons with an energy from 0.01 to 1 eV (wavelength from 10^{-10} to 10^{-9} m) are used. Neutrons are elementary particles without electrical charge and with the mass of $m_n = 1.675 \times 10^{-24}$ g or $1840 m_e$ (m_e being the mass of electron). Because of the relatively high mass of the neutron, the neutron radiation of a given wavelength has a very small energy ($E = h^2 / 2m_n \lambda^2$, h being the Planck constant and $\lambda = h / m_n v$ is the de Broglie wavelength of the neutron having the velocity v) as compared to, e.g., X-rays or electrons of comparable wavelengths. This makes neutrons an ideal probe for studying sensitive materials, such as surfactant assemblies and biological macromolecules. In contrast with X-rays, which are scattered by the electron clouds surrounding atomic nuclei, the neutrons are

scattered by the atomic nuclei themselves. As a result, neutron scattering permits detection of light elements, such as H, C and N, which are difficult to detect with X-rays. Furthermore, since the neutron/nucleus scattering cross-section significantly varies with the atomic mass – for instance, hydrogen has a cross-section of $1.8 \times 10^{-24} \text{ cm}^{-2}$ while deuterium has a cross-section of $5.6 \times 10^{-24} \text{ cm}^{-2}$ – hence different isotopes can be distinguished. Neutron scattering proved to be quite a versatile tool for microstructural analysis of colloidal, polymer and surfactant systems [38–42].

In a typical small angle neutron scattering (SANS) experiment on steady-state sources, a collimated beam of neutrons is directed at the sample and the scattering angle, θ , is measured. Note that $\theta = \pi - 2\varphi$ where φ is the angle of incidence. From of the scattering angle, the scattering vector $\mathbf{q} = \mathbf{k}' - \mathbf{k}$ (where \mathbf{k} and \mathbf{k}' are the wave vectors of the incident and scattered waves, respectively; and $|\mathbf{k}| = |\mathbf{k}'| = 2\pi/\lambda$) is found,

$$q = \frac{4\pi}{\lambda} \sin \frac{\theta}{2} \quad (30)$$

and experimental data are usually represented as scattered intensity, $I(q)$ vs. q . Instrumentally accessible q -range determines the size range of scattering bodies in a sample that can be probed at a given instrument; the resolved length scale having the order of magnitude of $1/q$.

The scattered intensity can be expressed as

$$I(R, \theta) = \frac{I_0 \sigma(\theta)}{R^2} \quad (31)$$

where I_0 is the intensity of the incident neutron beam, R is the distance to the detector and $\sigma(\theta)$ is the differential scattering cross-section. It is this latter quantity that bears all the information on the shape and size of the scattering bodies in the sample. Correspondingly, the total scattering cross-section is $\sigma_{\text{tot}} = \int \sigma d\Omega = 2\pi \int \sigma(\theta) \sin \theta d\theta$, where Ω is the solid angle. In q -coordinates, the differential cross-section may be factorized as follows,

$$\begin{aligned} \sigma(q) &= b^2 \iint_{V_s} N_n(\mathbf{r}) N_n(\mathbf{r}') \exp[i\mathbf{q} \cdot (\mathbf{r} - \mathbf{r}')] d^3\mathbf{r} d^3\mathbf{r}' \\ &= \left\{ (w - w_0) \int_{V_s} \exp(-i\mathbf{q} \cdot \mathbf{R}) d^3\mathbf{R} \right\}^2 \\ &\quad \times \iint_{V_s} \langle N_p(\mathbf{r}) N_p(\mathbf{r}') \rangle \exp[i\mathbf{q} \cdot (\mathbf{r} - \mathbf{r}')] d^3\mathbf{r} d^3\mathbf{r}' \\ &= V_s V_p^2 N_p^2 (w - w_0)^2 \mathcal{P}(q) \mathcal{S}(q) \end{aligned} \quad (32)$$

where V_s is the volume of the sample exposed to the neutron beam, V_p is the volume of one scatterer, N_p is the number density of scatterers in the volume V_s , N_n is the number density of nuclei, b is the scattering length (also known as the scattering amplitude), w and w_0 are the

neutron scattering length densities (which are assumed to be uniform over the volume of the scattering body) for the sample and for the surrounding medium, respectively, $\mathcal{P}(q)$ is the form factor characterizing the scatterer geometry and $\mathcal{S}(q)$ is the structure factor characterizing the distribution of scatterers in the volume V_s . The neutron scattering length density for a molecular substance can be calculated as

$$w = \frac{\rho N_A}{M_w} \sum_i b_i \quad (33)$$

where ρ is the bulk density of the substance, M_w is its molecular weight, N_A is the Avogadro number, and b_i is the neutron scattering length for the i th atom (nucleus). Alternatively, one can simply take

$$w = \sum_i N_{ni} b_i \quad (34)$$

where N_{ni} is the number density of the i th atom. The neutron scattering length is an element-dependent quantity and its values for all chemical elements and their most common isotopes are known [43]. The scattering length characterizes the efficiency of the scattering process. If the incident neutron wave is described by the wave function $\psi_i = \exp(ikr)$, the wave scattered by an atomic nucleus will be $\psi_s = (b/r) \exp(ik'r)$. Provided that there is no interference between the incident and scattered waves, the probability of finding a scattered neutron at the distance r from the nucleus is $|b|^2/r^2$. Therefore, the total scattering cross-section $\sigma_{\text{tot}} = 4\pi|b|^2$ and the differential cross-section $\sigma = |b|^2$.

The form factor, $\mathcal{P}(q)$, takes into account the geometry of the scattering body and is defined as [44],

$$\mathcal{P}(q) = \left[\frac{1}{V_p} \int_{V_p} \exp(-i\mathbf{q} \cdot \mathbf{r}) d^3\mathbf{r} \right]^2 \quad (35)$$

Note that, in the present definition, the factor $w - w_0$ has been moved out of the integral because of constancy of the scattering length densities over the scatterer volume (cf. Eq. (32)). Analytical expressions for $\mathcal{P}(q)$ for many simple geometries can be obtained (see Table 1). For small q 's,

$$\begin{aligned} \text{Re} \int_{V_p} \exp(-i\mathbf{q} \cdot \mathbf{r}) d^3\mathbf{r} &\approx V_p \left(1 - \frac{1}{2V_p} \int_{V_p} (\mathbf{q} \cdot \mathbf{r})^2 d^3\mathbf{r} + \dots \right) \\ &= V_p \left(1 - \frac{1}{2} \langle q_x^2 x^2 + q_y^2 y^2 + q_z^2 z^2 \rangle + \dots \right) \\ &= V_p \left(1 - \frac{1}{6} q^2 r_g^2 + \dots \right) = V_p \exp\left(-\frac{q^2 r_g^2}{6}\right) \end{aligned} \quad (36)$$

whence the radius of gyration, r_g , of the scattering bodies can be found by plotting $\log I(q)$ vs. q^2 .

Table 1
Form factors for different geometries of the scattering body [44]

Geometry	Form factor
Solid sphere of radius r	$\mathcal{P}(q) = \left\{ \frac{3}{(qr)^3} [\sin(qr) - qr \cos(qr)] \right\}^2$
Thin rod of length L	$\mathcal{P}(q) = \frac{2}{qL} \int_0^{qL} \frac{\sin v dx}{x} - \left(\frac{2}{qL} \sin \frac{qL}{2} \right)^2$
Thin disk of radius r	$\mathcal{P}(q) = \frac{2}{(qr)^2} \left[1 - \frac{J_1(2qr)}{qr} \right]$ (J_1 being the Bessel function of the first order)
Gaussian coil with radius of gyration r	$\mathcal{P}(q) = \frac{2}{(qr)^4} \left[e^{-(qr)^2} + (qr)^2 - 1 \right]$

The structure factor, $\mathcal{S}(q)$, is related to the particle-particle correlation function, $g(\mathbf{r})$, which characterizes the probability of finding a particle in the point \mathbf{r} provided that there is one at the origin [41],

$$\begin{aligned} \mathcal{S}(q) &= 1 + \frac{1}{V_s} \int_{V_s} [g(\mathbf{r}) - 1] \exp(-i\mathbf{q} \cdot \mathbf{r}) d^3\mathbf{r} \\ &= 1 + \frac{4\pi}{qV_s} \int_0^\infty [g(r) - 1] \sin(qr) r dr \end{aligned} \quad (37)$$

To retrieve information on the size and shape of scatterers in the sample in study, experimental data $I(q)$ vs. q are approximated by theoretical curves calculated using different form factors (and characteristic lengths) until a suitable agreement is achieved.

Small-angle neutron scattering is used in studies on surfactant aggregation for the determination of the structure and composition of micelles or vesicles on length scales of 1 to 1000 nm and for density profiling of polymer and surfactant layers adsorbed to the surfaces of colloidal particles [45–49].

2.2.4. Neutron reflectivity

Neutron reflectivity, in combination with isotopic substitution, is a powerful method for studying the structure and composition of adsorbed layers at the gas/liquid and liquid/solid interfaces. This method affords information about the density and composition profiles the adsorbed layers in the direction normal to the interface; the accessible thickness range being 1 to 500 nm. Neutron reflectivity provides a level of selectivity not directly available in other techniques, such as ellipsometry and X-ray reflectivity [50,51].

Consider a simple optical model consisting of a substrate (phase 3) covered by a thin film (phase 2) and being in contact with an ambient medium (phase 1). The refractive indices of each of the phases with respect to the neutron radiation are calculated as

$$n_i = 1 - \frac{\lambda^2 w_i}{2\pi} \quad (38)$$

where w_i is the scattering length density of the i th phase. The last formula directly follows from the fact that

$$n_i = \frac{v_i}{v_0} = \left(\frac{E - U}{E} \right)^{1/2} \approx 1 - \frac{U}{2E} \quad (39)$$

where v_i and v_0 are the velocities of neutrons in the i th phase and in vacuum, respectively, $E = m_n v_0^2 / 2 = \hbar^2 / 2m_n \lambda^2$ is the kinetic energy of the neutron in vacuum, and U is the volume-average potential of the neutron/nuclei interaction in the i th phase,

$$U = \frac{\hbar^2 n_i b}{2\pi m_n} = \frac{\hbar^2 w_i}{2\pi m_n} \quad (40)$$

The latter formula is easily obtained by treating the potential, U , as a weak perturbation, in which case the scattered wave can be approximated by

$$\begin{aligned} \psi_s(\mathbf{r}) &\approx \exp(i\mathbf{k} \cdot \mathbf{r}) + \frac{2\pi m_n}{\hbar^2} \\ &\times \frac{\exp(i\mathbf{k} \cdot \mathbf{r})}{r} \int U(\mathbf{r}') \exp[i(\mathbf{k} - \mathbf{k}') \cdot \mathbf{r}'] d^3\mathbf{r}' \end{aligned} \quad (41)$$

This is known as the Born approximation. Accordingly, the scattering length will be

$$b \approx \frac{2\pi m_n}{\hbar^2} \int U(\mathbf{r}) \exp(-i\mathbf{q} \cdot \mathbf{r}) d^3\mathbf{r} \quad (42)$$

For small velocities of the incident neutrons, $\exp(-i\mathbf{q} \cdot \mathbf{r}) \approx 1$, and hence

$$b \approx \frac{2\pi m_n}{\hbar^2} \int U(\mathbf{r}) d^3\mathbf{r} \approx \frac{2\pi m_n U a^3}{\hbar^2} \quad (43)$$

where a is the characteristic potential decay length. On recalling that $b/a^3 = w$, Eq. (40) is immediately arrived at.

Once the refractive indices of the interfacial film and the adjacent bulk phases are known, the neutron reflectivity, $\mathcal{R}(q)$, can be expressed through the Fresnel coefficients, R_{ij} ($i, j = 1, 2, 3$) (see Eq. (14)),

$$\mathcal{R}(q) = \frac{R_{12}^2 + R_{23}^2 + 2R_{12}R_{23} \exp(-i\beta)}{1 + R_{12}^2 R_{23}^2 + 2R_{12}R_{23} \exp(-i\beta)} \quad (44)$$

where

$$\beta = \frac{4\pi l}{\lambda} n_2 \cos \varphi_2 = \frac{4\pi l}{\lambda} n_2 \sin \left(\frac{\pi}{2} - \varphi_2 \right) \approx ql \quad (45)$$

for incidence angles close to $\pi/2$. The numbering of the phases is the same as in Fig. 3. In this way, one can determine the film thickness, l , by measuring the $\mathcal{R}(q)$ vs. q dependence [52].

In practice, a somewhat different approach is more convenient. Provided that the scattering length density, $w(\mathbf{r})$,

changes only in the direction normal to the interface (i.e., the z -direction), the reflectivity, $\mathcal{R}(q)$, can be linked to $w(z)$ by using Eqs. (32), (40) and (42),

$$\begin{aligned}\mathcal{R}(q) &= \frac{k}{-\mathbf{k} \cdot \mathbf{n} S} \int \sigma d\Omega \\ &= \frac{k}{-\mathbf{k} \cdot \mathbf{n} S} \int \left\{ w^2 \iint \exp[i\mathbf{q} \cdot (\mathbf{r} - \mathbf{r}')] d^3\mathbf{r} d^3\mathbf{r}' \right\} d\Omega \\ &= \frac{16\pi^2}{q^2} \left| \int_{-\infty}^{+\infty} w(z) \exp(-iqz) dz \right|^2\end{aligned}\quad (46)$$

where S is the interfacial area exposed to the neutron beam.

The scattering length density profile, $w(z)$, is represented by an appropriate model function. The fact that $w(z)$ can be manipulated by isotopic substitution is often used to minimize uncertainty concerning the choice of the best structural model that would fit to the measured $\mathcal{R}(q)$ vs. q profile. Inasmuch as the determination of the structure and composition of the adsorbed layer is model-dependent, it is of paramount importance to be able to combine reflectivity profiles for a range of solutions of the same chemical composition but different isotopic composition. A comprehensive review of the subject is available [53].

When using different fronting and backing materials for the same film the properties of which are to be determined, reflectivity data can be directly inverted to obtain $w(z)$. An example is shown in Fig. 5.

3. Dynamics of surfactant adsorption and surface tension relaxation

The rate of surfactant adsorption from a continuous bulk phase to a surface can be controlled by (i) transport of

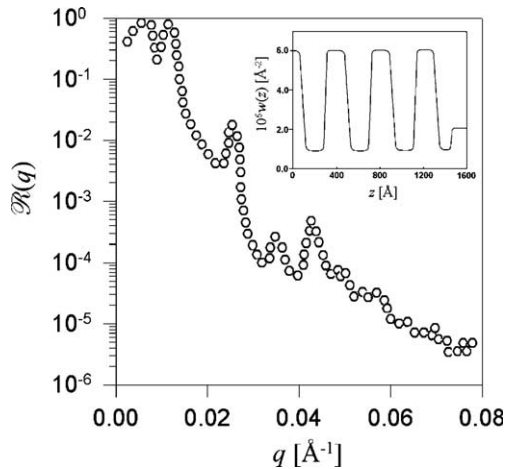


Fig. 5. Neutron reflectivity from a block copolymer film cast onto a silicon substrate. The scattering length density profile fitted to the reflectivity data is shown in the inset (redrawn from Ref. [51]).

surfactant molecules to the interfacial region, called the subsurface, (ii) transfer from the subsurface to the surface, which possibly involves reorientation and conformational changes of molecules, and (iii) by both of the above-mentioned factors simultaneously. Correspondingly, it is customary to distinguish diffusion-controlled, activation-controlled, and mixed kinetics [54].

3.1. Diffusion-controlled adsorption kinetics

Let us analyze the dynamics of surfactant adsorption to a freshly created liquid/vapour interface. As soon as a fresh interface is created, surfactant starts to migrate to that interface and adsorb thereto. The process continues until the equilibrium surface excess of surfactant is restored. In the course of this process, the interfacial tension will decrease – in accordance with the Gibbs law – following the surfactant adsorption. For the sake of simplicity, the interface is assumed to be planar. This assumption is valid if the principal radii of curvature of the interface are much greater than the characteristic diffusion length. With this assumption, the transport of surfactant from the bulk solution to the interface is described by the one-dimensional diffusion equation [55],

$$\frac{\partial c(x,t)}{\partial t} = D \frac{\partial^2 c(x,t)}{\partial x^2} \quad (47)$$

where $c(x,t)$ is the concentration of surfactant in solution at the distance x from the interface at time t , and D is the diffusion coefficient of surfactant in solution. The following initial condition for $c(x,t)$ can be specified:

$$c(x,0) = C_0 \quad (48)$$

where C_0 is the initial concentration of surfactant in the bulk solution. Besides that, the function $c(x,t)$ should satisfy the following boundary conditions,

$$D \frac{\partial c}{\partial x} \Big|_{x=0} = \frac{d\Gamma}{dt}$$

$$c(\infty, t) = C_0 \quad (49)$$

the first of which shows that the cumulative amount of surfactant transported to the liquid/vapour interface constitutes the surface excess, $\Gamma(t)$, at the latter, and the second says that the concentration of surfactant in remote solution regions is not affected by adsorption. In other words, the solution phase is considered as an infinite reservoir of surfactant. From Eqs. (47)–(49), one gets

$$\begin{aligned}\Gamma(t) &= \int_0^t dt \left[D \frac{\partial c}{\partial x} \Big|_{x=0} \right] = \int dt \int dx \left[\frac{\partial}{\partial x} \left(D \frac{\partial c}{\partial x} \right) \right] \\ &= \int dx \int dt \left(\frac{\partial c}{\partial t} \right) = \int_0^\infty [C_0 - c(x,t)] dx\end{aligned}\quad (50)$$

which is nothing other than the mass conservation constraint.

The surface excess of surfactant at the liquid/vapour is related to the concentration of surfactant near the interface,

$$\Gamma(t) = f \circ c(0, t) \quad (51)$$

and hence,

$$c(0, t) = f^{-1} \circ \left\{ \int_0^\infty [C_0 - c(x, t)] dx \right\} \quad (52)$$

where $f(c)$ describes the adsorption isotherm, and f^{-1} represents the inverse function of f . In the linear approximation, $\Gamma(t) = K_H c(0, t)$, where K_H is the Henry adsorption constant, and hence

$$c(0, t) = K_H^{-1} \int_0^\infty [C_0 - c(x, t)] dx \quad (53)$$

The solution of the diffusion Eq. (47) that satisfies the condition (48) and turns into $c(0, t)$ at the liquid/vapour interface is

$$c(x, t) = C_0 \operatorname{erf} \left(\frac{x}{2\sqrt{Dt}} \right) + \frac{1}{2\sqrt{\pi}} \int_0^t \frac{x}{\sqrt{D(t-t')}} \times \exp \left(-\frac{x^2}{4D(t-t')} \right) c(0, t') dt' \quad (54)$$

which holds true for any arbitrary function $c(0, t)$. By substituting Eq. (54) into the Eq. (53), a simple integral equation fixing $c(0, t)$ is obtained,

$$c(0, t) = \sqrt{\frac{D}{\pi K_H^2}} \left(2C_0 \sqrt{t} - \int_0^t \frac{c(0, t') dt'}{\sqrt{t-t'}} \right) \quad (55)$$

The latter is easily solved by Laplace's transform, which yields

$$c(0, t) = C_0 \left[1 - \exp(At) \operatorname{erfc}(\sqrt{At}) \right], \quad A = \frac{D}{K_H^2} \quad (56)$$

In the short-time limit ($t \ll 1/A$), one gets

$$\Gamma(t) \cong K_H c(0, t) \cong 2C_0 \sqrt{\frac{Dt}{\pi}} \quad (57)$$

Let us now derive the corresponding long-time asymptotics. The form of the latter depends on choice of the adsorption

isotherm. If the Langmuir adsorption isotherm is used, one can use the following expansion [56],

$$\begin{aligned} \phi(t) &\cong \phi_{\text{eq}} + (c(0, t) - C_0) \frac{d\phi}{dc} \Big|_{c=C_0} \\ &= \phi_{\text{eq}}^2 + c(0, t) \frac{d\phi}{dc} \Big|_{c=C_0}, \quad (t \rightarrow \infty) \end{aligned} \quad (58)$$

where

$$\phi(t) = \frac{\Gamma(t)}{\Gamma_m} \quad \text{and} \quad \phi_{\text{eq}} = \frac{\Gamma_{\text{eq}}}{\Gamma_m} = \frac{K_L C_0}{1 + K_L C_0} \quad (59)$$

where Γ_{eq} is the equilibrium surface excess, Γ_m is the monolayer capacity, and K_L is the Langmuir adsorption constant. Then, from the mass balance, it follows

$$\begin{aligned} \Gamma_m \left[\phi_{\text{eq}}^2 + c(0, t) \phi'(C_0) \right] \\ = \sqrt{\frac{D}{\pi}} \left(2C_0 \sqrt{t} - \int_0^t \frac{c(0, t') dt'}{\sqrt{t-t'}} \right) \end{aligned} \quad (60)$$

whence, by Laplace's transform, the following generating function, $L[s]$, is obtained,

$$\begin{aligned} L[s] = \frac{C_0 - \Gamma_m \phi_{\text{eq}}^2 \sqrt{s/D}}{s \left(1 + \Gamma_m \phi'(C_0) \sqrt{s/D} \right)} \cong \frac{C_0}{s} \\ \times \left[1 - \frac{\Gamma_m}{\sqrt{D}} \left(\phi'(C_0) + \frac{\phi_{\text{eq}}^2}{C_0} \right) \sqrt{s} + \dots \right], \quad (s \rightarrow 0) \end{aligned} \quad (61)$$

Finally, by inverse transform, the sought long-term asymptotics is arrived at,

$$\begin{aligned} c(0, t) = C_0 \left[1 - \frac{\Gamma_m}{\sqrt{\pi D}} \left(\phi'(C_0) + \frac{\phi_{\text{eq}}^2}{C_0} \right) \frac{1}{\sqrt{t}} + \dots \right] \\ \cong C_0 - \frac{\Gamma_{\text{eq}}}{\sqrt{\pi D t}} \quad (t \rightarrow \infty) \end{aligned} \quad (62)$$

and

$$\Gamma(t) = \frac{\Gamma_m K_L c(0, t)}{1 + K_L c(0, t)} \cong \Gamma_{\text{eq}} \left(1 - \frac{\Gamma_{\text{eq}}^2}{\Gamma_m K_L C_0^2 \sqrt{\pi D t}} \right) \quad (t \rightarrow \infty) \quad (63)$$

Now that the time-evolution of the surface excess is known, the dynamic surface tension can be readily calculated; for instance, by using the Frumkin equation,

$$\gamma(t) = \gamma_0 + \Gamma_m k_B T \ln \left(1 - \frac{\Gamma(t)}{\Gamma_m} \right) = \begin{cases} \gamma_0 - 2C_0 k_B T \sqrt{\frac{Dt}{\pi}}, & (t \rightarrow 0) \\ \gamma_{\text{eq}} + \frac{\Gamma_{\text{eq}}^2 k_B T}{C_0 \sqrt{\pi D t}}, & (t \rightarrow \infty) \end{cases} \quad (64)$$

where surface excess is expressed in m^{-2} and concentration in m^{-3} .

3.2. Activation-controlled adsorption kinetics

Let the adsorption kinetics obey the Langmuir–Hinshelwood equation,

$$\frac{d\phi}{dt} = [k_+ C_0 (1 - \phi) - k_- \phi] \exp(-B\phi) \quad (65)$$

where k_+ and k_- are the adsorption and desorption rate constants, and B is an empirical parameter taking into account adsorbate–adsorbate interactions in the adsorbed layer. Integration of Eq. (65) yields

$$\ln\left(1 - \frac{\phi(t)}{\phi_{\text{eq}}}\right) + \sum_{i=1}^{\infty} \frac{(-B)^i}{i \cdot i!} [\phi_{\text{eq}} - \phi(t)]^i + \frac{C_0 k_+ t}{\phi_{\text{eq}} \exp(B\phi_{\text{eq}})} = \text{const} \quad (66)$$

This is a transcendental equation defining $\phi(t)$. Once $\phi(t)$ is determined, the surface tension dynamics can then be calculated by the equation,

$$\gamma(t) = \gamma_0 + \Gamma_m k_B T \ln[1 - \phi(t)] \quad (67)$$

Further, on taking into account that $\phi(t) \rightarrow \phi_{\text{eq}}$ as $t \rightarrow \infty$, the following asymptotic formulas are arrived at,

$$1 - \frac{\phi(t)}{\phi_{\text{eq}}} \sim \exp\left(-\frac{C_0 k_+ t}{\phi_{\text{eq}} \exp(B\phi_{\text{eq}})}\right), \quad (t \rightarrow \infty) \quad (68)$$

and

$$\gamma(t) = \gamma_0 + \Gamma_m k_B T \times \ln\left\{1 - \phi_{\text{eq}} \left[1 - \exp\left(-\frac{C_0 k_+ t}{\phi_{\text{eq}} \exp(B\phi_{\text{eq}})}\right)\right]\right\} \quad (69)$$

3.3. Mixed adsorption kinetics

In this case, a modified form of the Langmuir–Hinshelwood equation,

$$\frac{d\phi}{dt} = [k_+ c(0, t)(1 - \phi) - k_- \phi] \exp(-B\phi) \quad (70)$$

where C_0 has been replaced by $c(0, t)$, the concentration of surfactant in the vicinity of a non-equilibrated liquid/vapour interface, is coupled with the boundary condition,

$$\Gamma_m \frac{d\phi}{dt} = D \frac{\partial c}{\partial x} \Big|_s \quad (71)$$

expressing the surfactant flow continuity. It is easy to show that the diffusion-controlled kinetics and the activation-controlled kinetics are obtained as the limiting cases corresponding to, respectively, large and small values of the rate constants, k_+ and k_- [56,57]. Since k_+ and k_- are bound by the constraint that $K = k_+/k_-$, where K is the adsorption equilibrium constant, $c(0, t)$ can be written as,

$$c(0, t) = \frac{\exp(B\phi)}{k_+(1 - \phi)} \frac{d\phi}{dt} + \frac{\phi}{K(1 - \phi)} \quad (72)$$

For sufficiently large k'_s ($k_+ \gg DC_0/\Gamma_m^2$), the first term vanishes, and therefore, the magnitude of adsorption to the gas/liquid interface at any time is uniquely related to the concentration of adsorbate near the interface at the same time. This is a prerequisite for the diffusion-controlled adsorption regime. Conversely, for small k'_s , the derivative $d\phi/dt$ itself is small, and so is the gradient dc/dx near the interface. This is only possible if $c(0, t) \approx C_0$. Hence, in the case of small k'_s one returns to Eq. (65) corresponding to the activation-controlled adsorption regime.

3.4. Adsorption from micellar solutions

At concentrations above the critical micelle concentration (cmc), only a fraction of surfactant in solution is preserved in the monomer form while the rest is aggregated into micelles. The formation and decay of the micelles are the dynamic processes that influence the surface tension dynamic. The intensity of monomer–micelle interconversion in a solution containing monomers at the concentration c_1 and N -micelles (N being the aggregation number) at the concentration c_N can be successfully modelled by the function [57],

$$Q(\mathbf{r}, t) = [\text{cmc} - c_1(\mathbf{r}, t)][k_{N \rightarrow 1}(t)c_N(\mathbf{r}, t) + k_{1 \rightarrow N}(t)c_1(\mathbf{r}, t)] \quad (73)$$

where $k_{1 \rightarrow N}$ and $k_{N \rightarrow 1}$ are some kinetic parameters. Because of this interconversion, the diffusive flows of monomers and micelles become interrelated [57–59]

$$\begin{cases} \frac{\partial c_1}{\partial t} = D_1 \nabla^2 c_1 + Q \\ \frac{\partial c_N}{\partial t} = D_N \nabla^2 c_N - Q \end{cases} \quad (74)$$

where D_1 and D_N are the diffusion coefficients of the monomers and the micelles, respectively. Since diffusivity of micelles is limited because of their larger size, D_N is normally less than D_1 .

A somewhat different theoretical interpretation [60] of the surface tension relaxation kinetics in micellar solutions consists in considering the micelles as quasi-monodisperse aggregates of two sizes: large and small. In this way, the

existence of two relaxation processes, a fast one and a slow one, can be explained. During the fast process, the bigger micelles, called p -micelles, release a certain number of monomers and transform into the smaller ones, called q -micelles, without influencing the total number of micelles. During the slow process, both large and small micelles release monomers and the total number of micelles decreases. However, the overall exchange kinetics are still described by a system of second-order kinetic equations similar to those incorporated in Eqs. (73) and (74).

The above approach can be easily extended to a more general case of polydisperse micellar solutions. Let $\chi = \chi(N, \mathbf{r}, t)$ be the distribution of micelles by their aggregation numbers, N , such that

$$\int \chi dN = C_0 \quad (75)$$

For such a polydisperse system, the transport of surfactant is described by an equation of the type

$$\frac{\partial \chi(N, \mathbf{r}, t)}{\partial t} = D(N) \nabla^2 \chi(N, \mathbf{r}, t) + Q[\chi, N] \quad (76)$$

with the source function

$$Q[\chi, N] = \int \kappa(N, N') \{ \chi(N') - \bar{\chi}(N') \} dN' \quad (77)$$

where $\bar{\chi}$ is the equilibrium distribution of micelles and κ is the function describing the aggregation–disaggregation kinetics.

Usually, only monomers are assumed to be capable of adsorption, i.e.

$$\frac{d\Gamma}{dt} = -D(1) \mathbf{n} \cdot \nabla \chi(1, \mathbf{r}, t)|_S \quad (78)$$

where \mathbf{n} is the unit normal to the interface S .

The particular case of Eq. (74) is obtained by putting

$$\chi(N') = c_1(\mathbf{r}, t) \delta(1 - N') + c_N(\mathbf{r}, t) \delta(N - N')$$

$$\bar{\chi}(N') = \text{cmc} \delta(1 - N') + (C_0 - \text{cmc}) \delta(N - N') \quad (79)$$

where $\delta(x)$ is the Dirac delta function.

3.5. Adsorption of mixed surfactants

To address this case, it is convenient to use the free energy approach [61], the idea of which is to express the reduction in the surface tension caused by surfactant adsorption in terms of the changes in the interfacial free energy,

$$\begin{aligned} \gamma(x_1^b, x_2^b, \dots, x_N^b) - \gamma_0 \\ = \int_0^\infty \Delta F_V(x_1, x_2, \dots, x_N) dz + \Delta F_S(x_1^S, x_2^S, \dots, x_N^S) \end{aligned} \quad (80)$$

where F_V is the bulk contribution and F_S is the surface contribution to the free energy, and $x_i = x_i(z)$ and x_i^S are the

volume fractions of the i th component in solution and at the interface, respectively, and $x_i^b = x_i(\infty)$. In dilute nonionic surfactant systems, the surface contribution is the dominant one. Therefore, for calculation of the bulk contribution term, the zero-order approximation can be used,

$$\begin{aligned} \Delta F_V(x_1, x_2, \dots, x_N) = \Delta F_V^1(x_1) + \Delta F_V^2(x_1) + \dots \\ + \Delta F_V^N(x_N) \end{aligned}$$

$$\frac{a^3}{k_B T} \Delta F_V^i(x_i) = x_i \ln x_i - x_i - (x_i^b \ln x_i^b - x_i^b) - \bar{\mu}_i (x_i - x_i^b) \quad (81)$$

where the intermolecular interactions between different species are neglected. Here, a is the effective molecular size (assumed equal for all the species), and μ_i is the reduced chemical potential of the i th surfactant in the bulk.

At the interface, however, the volume fractions of surfactants are significantly higher than in the bulk, which necessitates the introduction of non-linear interaction terms,

$$\begin{aligned} \frac{a^2}{k_B T} \Delta F_S(x_1^S, x_2^S, \dots, x_N^S) = \sum_i x_i^S \ln x_i^S + \left(1 - \sum_i x_i^S \right) \\ \times \ln \left(1 - \sum_i x_i^S \right) - \sum_i \left\{ [\alpha_i + \bar{\mu}_i^S] x_i^S + \frac{1}{2} \beta_i (x_i^S)^2 \right\} \\ - \sum_{i < j} \varepsilon_{ij} x_i^S x_j^S \end{aligned} \quad (82)$$

where α_i is a parameter characterizing the adsorption affinity of the i th surfactant, $\bar{\mu}_i^S$ is the reduced chemical potential of this surfactant at the interface, β_i is the pairwise interaction parameter for alike molecules, and ε_{ij} is the pairwise interaction parameter for different molecules.

Given the above equations, one can simply deduce the equation of state,

$$\begin{aligned} \gamma(x_1^b, x_2^b, \dots, x_N^b) - \gamma_0 = \Gamma_m k_B T \left[\ln \left(1 - \sum_i x_i^S \right) \right. \\ \left. + \frac{1}{2} \sum_i \beta_i (x_i^S)^2 + \sum_{i < j} \varepsilon_{ij} x_i^S x_j^S \right] \end{aligned} \quad (83)$$

where the monolayer capacity $\Gamma_m = a^{-2}$. Eq. (83) represents a generalized form of the Eq. (67). In equilibrium, x_i^S and x_i^b are linked to each other via the corresponding adsorption isotherm equations.

To describe the kinetics of adsorption and surface tension relaxation in a multicomponent system, transport equations for each component must be specified in addition to Eq. (83). For single-surfactant (binary) systems, this problem has already been addressed in the previous sections, and the

extension of the results obtained there to the case of many-surfactant mixtures is rather straightforward.

4. Intermolecular interactions in aggregated surfactant

The tendency of the free energy to be a minimum is the driving force of surfactant aggregation. In general, there may be quite a few sources, such as transfer free energy of surfactant tails, deformation free energy of surfactant tails, core-water interfacial free energy, head group sterical interactions, head group dipole interactions, head group ionic interactions, free energy of mixing of surfactant tails, etc., which all contribute to the overall energy balance. When surfactant adsorption is concerned, adsorbate–adsorbent interactions further come into play. A remarkable fact is that the utmost complexity of surfactant aggregation phenomena harmonically coexists with grossly simplified theoretical models used in their analysis. For instance, the interaction energy between the surfactant species in mixed micelles and adsorbed layers can be easily estimated using the pseudophase separation model [62,63] based on the largely empirical regular solution theory [64]. In this model, the cmc of a binary surfactant system is related to the cmc's of individual components by

$$\frac{1}{\text{cmc}} = \frac{\phi_1}{\text{cmc}_1} \exp(-\beta x_1^2) + \frac{\phi_2}{\text{cmc}_2} \exp(-\beta x_2^2)$$

$$\phi_i = \frac{c_i}{c_1 + c_2} \quad (i = 1, 2)$$

$$x_1 + x_2 = 1 \quad (84)$$

where c_i is the monomer concentration of the i th surfactant in solution at cmc, x_i is the mole fraction of the i th surfactant in micelles, and β is the interaction parameter sought. By determining the cmc of mixed surfactant for a number of differing c_i 's with the aid of light scattering or surface tension titration, the interaction parameter and the micelle composition can be calculated from Eq. (84). Fig. 6 shows a typical set of experimental data enabling the determination of the interaction parameter in a binary surfactant mixture.

The existence of adsorbate–adsorbate interactions is necessarily reflected in the mathematical form of the adsorption isotherm, $\Gamma = \Gamma(c, T)$, and the equation of state, $\gamma = \gamma(\Gamma, T)$, for the adsorbed surfactant. The most common form of the adsorption isotherm is

$$\phi = \left\{ 1 + \frac{1}{Kc} \exp \left[f(\phi) - \frac{E(\beta)\phi}{k_B T} \right] \right\}^{-1} \quad (85)$$

where $f(\phi) = 0$ for the Langmuir, Frumkin, and Fowler–Guggenheim isotherms, and $f(\theta) = \theta/(1-\theta)$ for the Hill-de-Boer isotherm. In Eq. (85), c is the bulk concentration of surfactant, $E(\beta)$ is the energy of lateral interactions and K

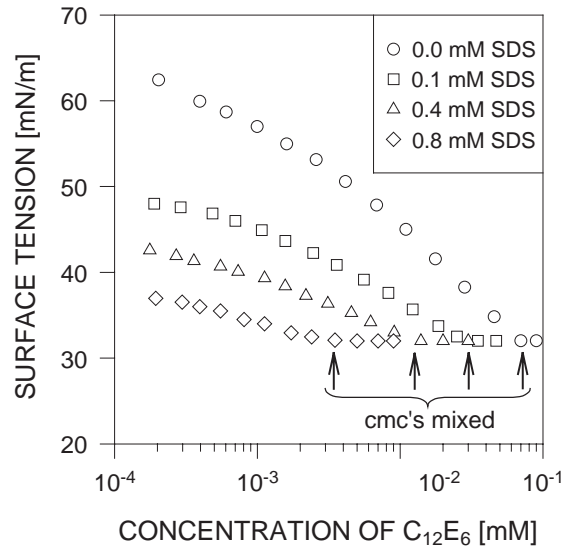


Fig. 6. Use of surface tension titration for the determination of cmc values in $C_{12}E_6$ /SDS mixed surfactant solutions in 0.1 M NaCl. The cmcs of pure $C_{12}E_6$ and SDS are 0.08 mM and 1.0 mM, respectively. The interaction parameter $\beta = -3.4$ indicating attractive interaction between $C_{12}E_6$ and SDS molecules (adapted from Ref.[63]).

is a parameter known as the adsorption equilibrium constant. It should be noted that, even though functional forms of adsorption isotherms that can be found in the literature are legion, the abovementioned adsorption isotherms are nearly the only isotherms that afford a solid statistical–mechanical substantiation and comprehensible equations of state.

It has been reported that strong lateral interactions between adsorbate molecules in non-ionic surfactants of the C_nE_m type may render the Langmuir isotherm inadequate [57,65,66]. The role of lateral interactions in C_nE_m surfactants also was studied by Nikas et al. [67] who managed to derive a rather general equation of state allowing quite accurate predictions of the static surface tension in composite mixtures.

Although the energy of lateral interactions can in principle be related to the interaction parameter, β , such a relation would be of little practical use because β itself is usually unknown. For that reason, $E(\beta)$ is directly evaluated by fitting a model isotherm to experimental adsorption data. For instance, by using the Frumkin isotherm,

$$\phi = \frac{Kc}{Kc + \exp[E(\beta)\phi/k_B T]} \quad (86)$$

in combination with the Gibbs equation,

$$\gamma(c) = \gamma_0 - \Gamma_m k_B T \int_0^c \frac{\phi(c)}{c} dc \quad (87)$$

one can evaluate $E(\beta)$ from surface tension titration data (Fig. 7).

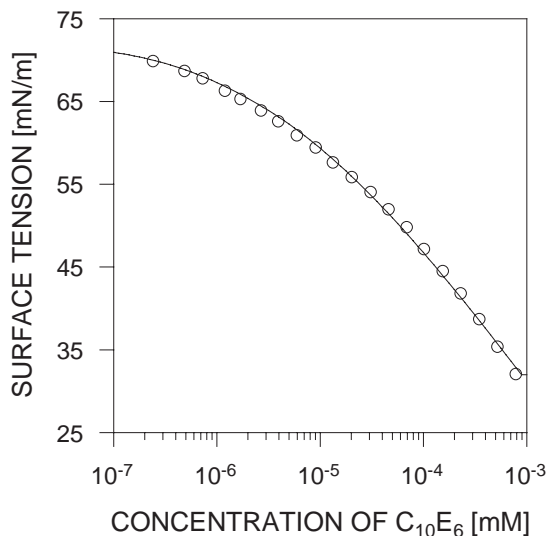


Fig. 7. Experimental surface tension titration data (O) for $C_{10}E_6$ surfactant and the best-curve calculated using Eqs. (86) and (87) with the following parameters: $K=1.53 \times 10^6 \text{ dm}^3/\text{mol}$; $\Gamma_m=1.78 \text{ nm}^{-2}$; and $E(\beta)=3.91 k_B T$.

If the lateral interaction are weak, so that $|E(\beta)| \ll k_B T$, the exponent in Eq. (86) can be linearized, making it possible analytical integration in Eq. (87), which gives

$$\gamma(c) = \gamma_0 - \Gamma_m k_B T \left\{ \ln(1 + Kc) - \frac{E(\beta)}{2k_B T} \left(\frac{Kc}{1 + Kc} \right)^2 \right\} \quad (88)$$

The latter equation represents a particular case of Eq. (83).

5. A review of experimental studies on the dynamics and structure of surfactant layers

The most powerful experimental methods for determination of the structure of surfactant layers are specular reflection of X-rays and neutrons, and to a lesser extent, ellipsometry. Neutron reflection permits direct determination of the dynamic surface excess and can be made chemically specific via deuterium-contrasting of the target compound. Ellipsometry also permits determination of the dynamic surface excess but does not provide any chemically specific information.

The structure of fluorinated nonionic surfactants of the type $\text{CH}_3(\text{CF}_2)_n\text{CH}_2\text{O}(\text{C}_2\text{H}_4\text{O})_m\text{CH}_3$ at the air/water interface was studied by neutron reflectivity [68] and it was demonstrated that surface coverage values derived from neutron reflectivity data are consistent with those measured tensiometrically. Another type of fluorinated polyhydroxy surfactants, tris(hydroxymethyl)acrylamidomethane-derived telomer bearing a perfluorohexyl hydrophobic chain, was studied using tensiometry, neutron reflection and SANS [69].

The structure of monolayers formed at the air/water interface by alkyltrimethylammonium bromides, $(\text{C}_n\text{H}_{2n+1})(\text{CH}_3)_3\text{NBr}$, ($C_n\text{TAB}$, with $n=10$ to 18) was studied using ellipsometry and neutron reflection [70–73]. It was found that increasing the length of the hydrocarbon chain results in a significant compaction of the hydrophobic part of the adsorbed layer. At the same time, the thickness of the layer changes only slightly. Short-chain members were found to form thick and disordered layers whereas long-chain members form more dense layers with a well-defined hydrophobic region contiguous to the head group region. The hydrophobic region represents a hydrocarbon melt. This behaviour demonstrates increasing significance of the chain–chain interaction compared to the head–water interaction along the homological series.

The structure of hexadecyltrimethylammonium bromide ($C_{16}\text{TAB}$) layers at the silica/water interface was studied by neutron reflection [74]. The thickness of the adsorbed layer was 34 Å, indicating that there actually was a bilayer formed. At the higher surfactant concentrations, the authors succeeded to resolve the structure of the bilayer into head and chain regions, but this distinction disappeared at the lower concentrations, whence a conclusion was drawn that the bilayer formation starts from the formation of small islands of surfactant on the surface.

The adsorption of cetylpyridinium bromide from aqueous solutions to the silica surface was studied by AFM and optical reflectometry [75]. It was observed that, at a low ion strength, the adsorption was extremely slow and that the addition of salt significantly speeded up the adsorption process. Slow adsorption kinetics were explained by the formation of surface aggregates which had been directly imaged with AFM. Indeed, the aggregation speed should increase with increasing the ion strength, both due to the electrical double layer contraction and due to counterion binding. This is also consistent with the fact that the cmc of cetylpyridinium bromide decreases upon the addition of salt. The effect of pH on the adsorption kinetics also was studied and it was reported that, in the presence of a background electrolyte, pH changes have little effect on the adsorption. Conversely, in the absence of electrolyte, the adsorption increased with pH as expected, but it was suggested that these increases were primarily due to increased ionic strength (better electrostatic shielding) and not due to increased charge on the substrate.

The adsorption of alkanediyl-bis(dodecyldimethylammonium bromide)-type gemini surfactants to a silica substrate was investigated using optical reflectometry and AFM [76]. The adsorption isotherms and kinetics of adsorption were determined for spacer sizes of 2, 3, 4, 6, 8, 10, and 12. The maximum surface excess was found to correlate strongly with the size of the spacer group, the smallest spacer size yielding the largest surface excess. In the case of surfactants with the shorter spacers, soft-contact AFM imaging performed by probing the surfactant layer with the AFM tip applied with a normal force set below the layer rupture limit

revealed the presence of flattened ellipsoidal aggregates on the surface. However, the internal structure of the surface aggregates remains uncertain.

The structure of alkyl ethers of polyethylene glycol monolayers was intensively studied by neutron reflection and a number of systematic trends identified [77,78]. Thus, the effective thickness of the hydrocarbon region was found to be significantly less the length of the fully extended hydrocarbon chain. Changes in the density of the hydrocarbon region were similar to those found for CTABs.

Transient behaviour of $C_{10}H_{21}(OC_2H_4)_8OH$ surfactant at an expanding air/water interface was studied by means of external-reflection Fourier transform infrared spectroscopy (ERFTIR) in an overflowing cylinder experiment [79]. EFTIR, as a form of vibrational spectroscopy, allows identification of different molecular species at the interface on the basis of their vibration spectra, and therefore, has the potential to measure quantitatively the surface coverage and composition in pure and mixed monolayers. Additional structural information can be retrieved from the peak shifts and the polarisation dependence of band intensities. Another variant of vibrational spectroscopy uniquely suited for measuring the vibrational spectrum of molecules at interfaces is vibrational sum frequency spectroscopy (VSFS) [80]. In VSFS, pulsing light from two superimposed laser beams produced by a coherent visible-light laser and a tunable IR laser are used to probe the interface. The high-intensity electric fields of the incident laser beams induce nonlinear polarization in the molecules at the interface. As a result, the molecules emit light at the sum of the two frequencies. If the wavelength of the IR laser corresponds to a molecular vibrational mode, a resonant enhancement in the sum frequency (SF) emission takes place. This serves as the identification basis. The surface specificity arises from the second-order nature of the SF response: the SF process is allowed by the symmetry rules only if the system has no inversion symmetry [81,82].

The structure of alkali dodecyl sulfate monolayers adsorbed to the air/water interface from lithium, sodium and cesium salts was studied using neutron reflection [83]. It was observed that the effective separation between the surfactant layer and the aqueous phase increases in the sequence Li to Na to Cs, and so does the monolayer capacity. This observation is obviously related to differences in the energies of counterion binding.

Small angle neutron scattering (SANS) was applied to study micellar growth in SDS [84], to monitor particle coalescence and SDS desorption from acrylic lattices during film formation [85], and to characterize mixed micelles formed by SDS and a sugar-based nonionic surfactant *n*-tetradecylmalono-bis(*N*-methylglucamide) $\{HOCH_2[CH(OH)]_4CH_2N(CH_3)CO\}_2CH-n-C_{14}H_{29}$ [10]. The aggregation behaviour of SDS in electrolytic solution

with a high ion strength was studied with cryo-TEM, SANS, dynamic light scattering, and time-resolved fluorescence quenching measurements, and a variety of aggregate structures, from broad band-like or lace-like aggregates to multiconnected threads, were discovered [86]. Adsorption of SDS and mixed SDS/ $C_{12}E_6$ surfactants at the oil/water interface in aqueous hexadecane emulsions was studied using SANS in combination with H/D isotopic substitution [87].

As has already been mentioned, surfactant adsorption at hydrophilic surfaces is often accompanied by interfacial aggregation [32,75,76,88]. As a consequence of this, several characteristic regimes may be identified in the adsorption process. In the case of ionic surfactants [75,76], the first regime taking place at low surfactant concentrations can be considered as a normal ion-exchange process which is driven by the entropy and electrostatic attraction to the oppositely charged solid surface. This regime lasts until the bulk surfactant concentration is increased up to the so-called hemimicelle concentration. At this point, which marks the onset of the second adsorption regime, the hydrophobic tails of the adsorbed surfactant molecules start to act as nucleation points for further surfactant adsorption. As a result, a marked increase in adsorption is observed, eventually leading to the surface charge reversal. A further increase in the bulk surfactant concentration up to the critical surface aggregation concentration (csac) causes a sharp increase in the adsorption due to the formation of admicelles. The term “admicelle” is used to describe adsorbed monomer aggregates with head groups facing both toward the surface and into the solution; incomplete bilayers and surface-adsorbed micelles are included in this definition. The formation of admicelles can be regarded as the third adsorption regime, in which the adsorption is driven predominantly by hydrophobic forces, i.e., the same forces that drive the micellization in solution. Depending on the system under investigation, the csac lies typically between one-third and two-thirds of the cmc. Further increases in the bulk surfactant concentration have no effect on the adsorption.

For nonionic surfactants [32,88], a similar sharp increase in the adsorption is observed when the csac is reached (see Fig. 8). Initially, as the csac is being approached, a layer composed of discrete surface aggregates with the thickness corresponding to that of a normal bilayer is formed. The number density and the lateral dimensions of the primary aggregates increase with increasing the bulk surfactant concentration, eventually leading to formation of a coherent bilayer or a periodic array of discrete admicellar structures [88] (see, for example, Fig. 9). Morphologies of a variety of such surface structures have been characterized with AFM [75,76,88–95].

One distinctive property of surfactants is their ability to form liquid crystalline phases. Thus, most lipids such as glycerol monooleate form bicontinuous cubic liquid crystalline phases essentially insoluble in water. In many respects, liquid crystals behave as fluids, even though they possess

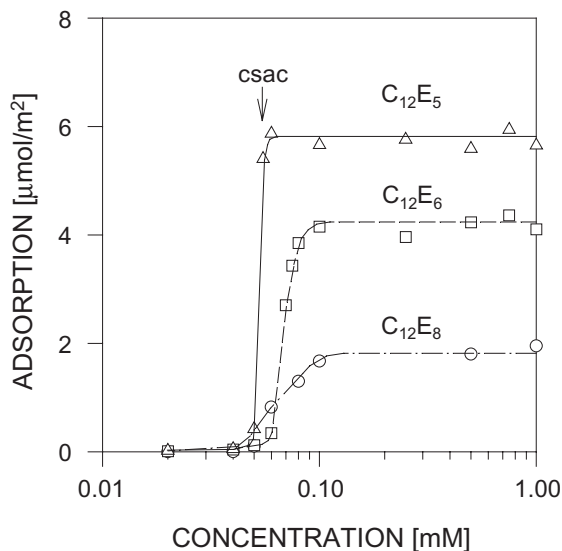


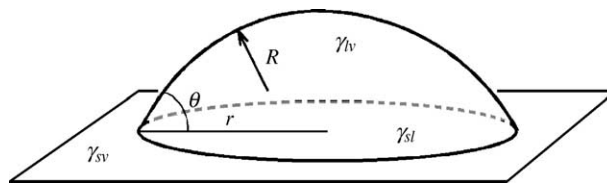
Fig. 8. Adsorption behaviour of C_nE_m surfactants on the silica surface near their critical surface aggregation concentration (csac) (redrawn from Ref. [32]).

more ordered structures than ordinary liquids. Cryo-TEM and small-angle X-ray scattering (SAXS) are the primary tools for the structural studies of liquid crystals [96–101]. The basic building blocks of the bicontinuous cubic phase are the lipid bilayers contorted into the shape of infinite periodic minimal surfaces. With such an arrangement, the average curvature of the bilayer at any point is zero, which minimizes stress and excess free energy of the cubic phase [96].

6. Wetting enhancement by surfactants

6.1. Thermodynamic consideration

Let us consider a small liquid drop of surfactant solution sitting at a partly wettable solid substrate,



Then, there are three interfaces contributing to the total excess free energy of the system shown,

$$F = F_{lv} + F_{sl} + F_{sv} \tag{89}$$

There exists an additional contribution, F_{svl} , from the three-phase contact line where all the three interfaces intersect. However, the corresponding correction is only significant for sub-micron size drops.

In the absence of the gravity effects, the lv interface has the shape of a spherical cap, and then

$$F_{lv} = \gamma_{lv}S_{lv} = 2\pi R^2\gamma_{lv}(1 - \cos\theta)$$

$$F_{sl} = \gamma_{sl}S_{sl} = \pi R^2\gamma_{sl}\sin^2\theta$$

$$F_{sv} = \gamma_{sv}S_{sv} = \text{const} - \pi R^2\gamma_{sv}\sin^2\theta \tag{90}$$

R being the curvature radius of the lv interface.

The value of θ corresponding to the minimum F is found from the equation,

$$\frac{dF}{d\theta} = 0 \tag{91}$$

taking into account that the volume, V , of the drop is constant and the radius, R , of the drop is related to the contact angle,

$$R(\theta) = \left(\frac{3V}{\pi(2 - 3\cos\theta + \cos^3\theta)} \right)^{1/3} \tag{92}$$

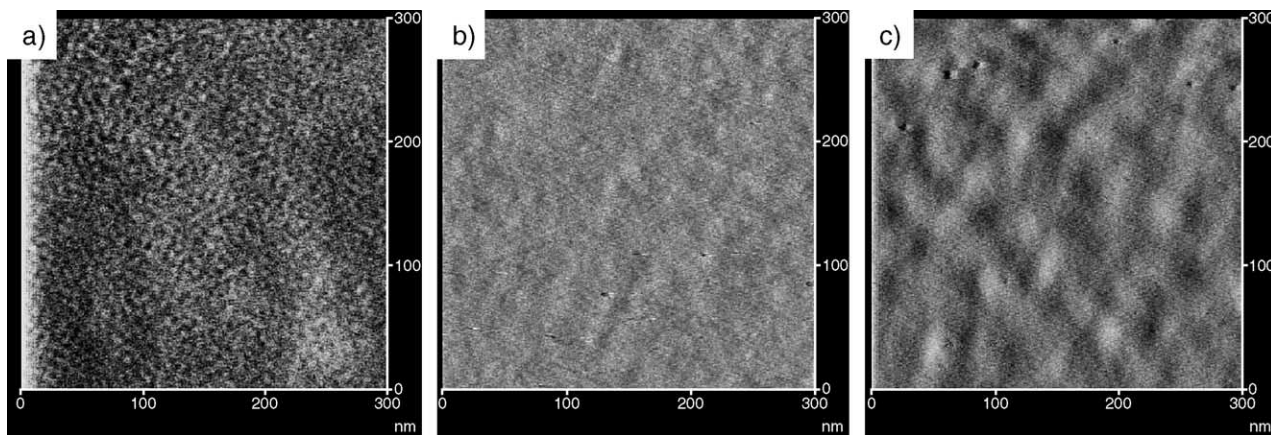


Fig. 9. AFM images of $C_{12}E_8$ surfactant layers adsorbed onto $\text{HS}(\text{CH}_2)_{16}\text{OH}/\text{HS}(\text{CH}_2)_{16}\text{CH}_3$ thiol-coated gold substances with differing levels of hydrophobicity: (a) 50% alkylated, (b) 75% alkylated, and (c) 100% alkylated. On the first two substrates, bilayers are formed, and on the third, most hydrophobic, substrate, a monolayer is formed (from Ref. [88]).

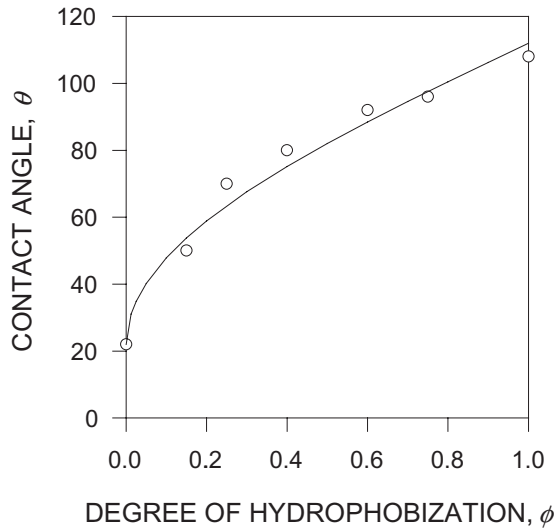


Fig. 10. Contact angle of water on mixed HS(CH₂)₁₆ OH/HS (CH₂)₁₆CH₃ thiol-coated substrates. The solid line represents the reference curve $\theta = \theta_0 + \arccos(1 - \phi)$ obeying the Young–Dupré equation (adapted from Ref. [102]).

After some basic arithmetics, one arrives at,

$$\cos\theta = \frac{\gamma_{sv} - \gamma_{sl}}{\gamma_{lv}} \quad (93)$$

This relation is known as the Young–Dupré equation.

It is clear that high-energy substrates, which are characterized by a high value of γ_{sv} , will be readily wettable by most liquids. In contrast, low-energy substrates are only wettable by liquids whose own surface tension, γ_{lv} , is low enough. Hydrophobization of substrates reduces the energy gained due to hydration, thus leading to higher γ'_{sl} s. Accordingly, the contact angle increases with increasing the degree of hydrophobization (see Fig. 10).

Since surfactants have been shown to reduce γ_{lv} s, and often γ_{sl} as well, they promote wetting. The equilibrium contact angle between a solid surface and a drop of surfactant solution is an ascending function of surfactant concentration, c ,

$$\begin{aligned} \cos\theta(c) &= \frac{\gamma_{sv} - \gamma_{sl}(c)}{\gamma_{lv}(c)} = \frac{\gamma_{sv} - \gamma_{sl}(0) + k_B T \int \Gamma_{sl}(c) d\ln c}{\gamma_{lv}(0) - k_B T \int \Gamma_{lv}(c) d\ln c} \\ &= \cos\theta(0) \left\{ 1 + \frac{k_B T}{\gamma_{lv}(0)} \int [\Gamma_{sl}(c) + \Gamma_{lv}(c)] d\ln c \right. \\ &\quad \left. + \dots \right\} > \cos\theta(0) \end{aligned} \quad (94)$$

i.e. the addition of surfactant leads to a decrease in the contact angle, $\theta(c) < \theta(0)$. This explains the wetting-enhancing effect of surfactants.

6.2. Dynamics of surfactant-induced drop spreading

Consider a small drop of surfactant solution spreading over a smooth solid substrate. In the creeping flow

regime, the spreading rate is determined by the momentary balance between the spreading tension and the viscous drag (see Fig. 11).

Let the spreading rate be low enough to maintain γ_{lv} and γ_{sl} at their equilibrium values. From a hydrodynamic viewpoint, this situation is characterized by simultaneously small Reynolds (Re), Bond (Bo) and Schmidt (Sc) numbers. If these conditions are satisfied, the Voinov–Hoffman–Tanner law [103] applies,

$$\frac{dr}{dt} \propto \frac{\gamma_{lv}}{\eta} \theta (\theta^2 - \theta_{eq}^2) \quad (95)$$

where θ is the dynamic contact angle, θ_{eq} is the equilibrium contact angle determined by the Young–Dupré Eq. (93) (it is assumed that $\theta_{eq} \neq 0$). Taking into account that, under the specified conditions, the dynamic contact angle and the spreading radius are linked to each other as follows,

$$\theta(t) \approx \frac{4V}{\pi r^3(t)} \quad (96)$$

one gets,

$$\frac{dr}{dt} \propto \frac{\gamma_{lv} V^3}{\eta r^3} \left(\frac{1}{r^6} - \frac{1}{r_\infty^6} \right) \quad (97)$$

Therefore, if $V^{1/3} \ll r \ll r_\infty$, the spreading radius increases with time as $r(t) \propto t^{1/10}$, and correspondingly, the contact angle decreases as $\theta(t) \propto t^{-3/10}$ [103].

The observed drop spreading dynamics are often in conflict with the Voinov–Hoffman–Tanner law, especially in the case of surfactant solutions spreading over hydrophobic substrates. This is explained by complexity of surfactant transport and adsorption kinetics which have been totally neglected in Eq. (95). In order to get a better understanding of the problem, let us examine the force balance at a curved interface separating two immiscible fluids, α and β , containing a surfactant. If the interface and adjacent phases are in equilibrium, the force balance is established by the Laplace formula,

$$p_\alpha - p_\beta = \gamma_{\alpha\beta} \left(\frac{1}{r_1} + \frac{1}{r_2} \right) \quad (98)$$

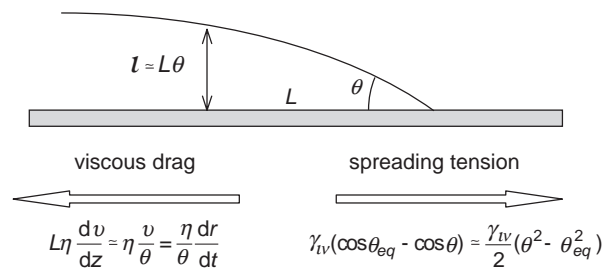


Fig. 11. The force balance near the margin of a liquid drop spreading over a solid substrate. It is assumed that $\max\{\theta, \theta_{eq}\} \ll 1$ and that the no-slip boundary condition holds at the solid/liquid interface.

where r_1 and r_2 are the principal curvature radii of the $\alpha\beta$ interface, and p_i ($i=\alpha,\beta$) is the pressure in the phases α and β . In this case, in particular, the interface is characterized by a constant curvature. Now consider the same system in non-equilibrium conditions, which may be the case if the adsorption of surfactant is not yet completed or the interface is disturbed. In such a situation, given the complex geometry of the interface, uneven adsorption of surfactant may be expected for different areas of the interface. As an example, one can consider a drop of a surfactant solution deposited on a hydrophobic substrate. Because of the adsorption of surfactant to the substrate, the margin of the drop is more depleted of surfactant than its center. Accordingly, the surface tension close to the margin is higher than in the center. This produces an additional surface stress, called the Marangoni stress, forcing liquid to move in the radial direction so as the surface excess of surfactant over the interface be levelled off. In the case considered, the interfacial force balance may be written as follows,

$$\left\{ p_\alpha - p_\beta - \gamma_{\alpha\beta} \left(\frac{1}{r_1} + \frac{1}{r_2} \right) \right\} \mathbf{n} = (\eta_\alpha \mathbf{E}_\alpha - \eta_\beta \mathbf{E}_\beta) \cdot \mathbf{n} + \nabla_S \gamma_{\alpha\beta} \quad (99)$$

where η_i ($i=\alpha,\beta$) are viscosities of the fluids α and β , respectively, \mathbf{n} is the unit normal, and \mathbf{E}_i ($i=\alpha,\beta$) are the strain tensors related to velocity profiles in the fluids α and β ,

$$E_{ik} = \left[\nabla \mathbf{v} + (\nabla \mathbf{v})^T \right]_{ik} = \frac{\partial v_i}{\partial x_k} + \frac{\partial v_k}{\partial x_i} \quad (100)$$

Notice the new term, $\nabla_S \gamma_{\alpha\beta}$ (∇_S being the surface gradient) on the right-hand side of Eq. (99)—it is this term that takes into account the additional stress arising from the surface tension gradient. The tangential force associated with adsorption-related surface tension gradients is

$$\frac{\partial \gamma_{\alpha\beta}}{\partial \Gamma_{\alpha\beta}} \nabla_S \Gamma_{\alpha\beta} \quad (101)$$

Note that Eq. (99) is often written in a more compact form,

$$[[p]] \mathbf{n} - 2H \gamma_{\alpha\beta} \mathbf{n} = [[\mathbf{T} \cdot \mathbf{n}]] + \nabla_S \gamma_{\alpha\beta} \quad (102)$$

where \mathbf{T} stands for the viscous stress tensor and $2H$ stands for the mean curvature of the interface, and the brackets indicate the difference between adjacent phases. In nonequilibrium conditions, the curvature of the interface is no longer constant.

In order to calculate the gradient in the surface excess, $\Gamma_{\alpha\beta}$, of surfactant, the surfactant transport equation,

$$\frac{\partial c}{\partial t} + \nabla \cdot (c\mathbf{v}) = D \nabla^2 c \quad (103)$$

with appropriate boundary conditions reflecting surfactant adsorption dynamics and surfactant transport over the interface, must be solved simultaneously with the Navier–Stokes equation of fluid dynamics. This tremendously

complex problem involving moving boundaries is far beyond the scope of this article. It should only be mentioned that, as a matter of fact, the role of surface diffusion in surfactant redistribution in adsorbed layers usually is small compared to Marangoni flow. This can be demonstrated by simple estimates. For a diffusion-controlled adsorption process, the characteristic equilibration time can be estimated as

$$\tau_{\text{eq}} \propto \frac{1}{10^6 D} \left(\frac{\Gamma_m K_L}{1 + K_L c} \right)^2 \quad (104)$$

The latter estimate is obtained from the condition that the surfactant adsorbed needs to path through a diffusion zone, the thickness of which is increasing with time as $(Dt)^{1/2}$, and therefore, the following scaling relation holds, $c(D\tau_{\text{eq}})^{1/2} \simeq \Gamma(c)$. Let there exist a surface tension gradient, which sets the surface layer of solution into motion. The top layer transfers momentum to the underlying layer, the latter, in its turn, transfers it to the next layer, and so on. As a result, the surface flow, keeping its lateral direction, will develop in depth. To which depth does the surface flow develop by the time τ_{eq} ? For example, if $D=10^{-9} \text{ m}^2 \text{ s}^{-1}$ and $c=10^{-4} \text{ mol dm}^{-3}$, it takes around 1 s for an equilibrium to be attained. During this time, in an aqueous solution with $\rho=10^3 \text{ kg m}^{-3}$ and $\eta=10^{-3} \text{ Pa s}$ the depth of the surface flow reaches $(\eta\tau_{\text{eq}}/\rho)^{1/2} \sim 1 \text{ mm}$, i.e. quite a significant volume of liquid is set in motion. Thus, one comes to the conclusion that the Marangoni effect may significantly influence the dynamics of small drops of surfactant solutions [104]. The Marangoni effect also lies behind the so-called superspreading phenomenon observed for aqueous solutions of trisiloxane surfactants [105,106].

Surfactant adsorption and Marangoni flow at an expanding liquid interface in a falling water jet was studied by ellipsometry with simultaneous measurement of the velocity profile with the jet by laser Doppler velocimetry [107]. It was found that near the nozzle, where the surface expansion rate is the highest, the surface excess is the lowest. This causes rapid diffusional transport of surfactant to the surface and rapid convection on the surface. The surface excess increases in the downstream direction creating a Marangoni stress which decelerates the surface. The Marangoni effect is also responsible for thickening of thin films in dip-coating applications ubiquitous in industrial processing [108].

7. Effect of surfactants on the damping of capillary waves

Adsorbed surfactant films affect the dynamics of free interfaces. This means that certain properties of surfactant films can be studied by monitoring the corresponding changes in the interfacial dynamics. As an example, one can mention the damping of capillary waves at a liquid

surface containing an adsorbed surfactant film. The presented analysis largely follows the scheme outlined in Ref. [109]. Two limiting cases corresponding to a compressible and an incompressible films will be considered.

In the first case, it is assumed that the adsorbed film present at the liquid/vapour interface does not to confine the motion of the liquid. Let a plane wave be running in the x -direction on the xy -plane representing the liquid/vapour interface in study. The z -axis goes to the liquid phase. For potential flows, the velocity field in the liquid phase can be expressed as the gradient of a scalar function called the velocity potential, $\mathbf{v}=\nabla\Phi$. Let $\zeta(x,t)$ represent the vertical displacement of the interface from its equilibrium position. If the amplitude of the waves is much smaller than the wavelength, one has

$$v_x = v_y = 0; \quad v_z = \frac{\partial \zeta}{\partial t} = \frac{\partial \Phi}{\partial z} \quad (105)$$

The pressure in the liquid under the curved interface is found from the Laplace equation (Eq. (98)),

$$p = -\gamma \frac{\partial^2 \zeta}{\partial x^2} \quad (106)$$

where, again, it is assumed that $|\partial \zeta / \partial x| \ll 1$. On the other hand, the force balance at the interface demands

$$p = -\rho g \zeta - \frac{\partial}{\partial t} \int (\rho v_z) dz = -\rho \left(g \zeta + \frac{\partial \Phi}{\partial t} \right) \quad (107)$$

and hence,

$$\gamma \frac{\partial^2 \zeta}{\partial x^2} = \rho \left(g \zeta + \frac{\partial \Phi}{\partial t} \right) \quad (108)$$

By differentiating the latter equation by t and taking into account Eq. (105), the following equation is arrived at

$$\gamma \frac{\partial^2 \Phi}{\partial x^2} = \rho \left(g \frac{\partial \Phi}{\partial z} + \frac{\partial^2 \Phi}{\partial t^2} \right) \quad (109)$$

the solution of which has the form

$$\Phi = \Phi_0 \exp(-kz) \cos(kx - \omega t) \quad (110)$$

where

$$\omega^2 = k \left(g + \frac{\gamma}{\rho} k^2 \right) \quad (111)$$

For the capillary waves, $k \gg (\rho g / \gamma)^{1/2}$, and hence

$$\omega^2 = \frac{\gamma}{\rho} k^3 \quad (112)$$

Let us now calculate the damping coefficient. The latter is defined as

$$\varepsilon = -\frac{\langle dE/dt \rangle}{2\langle E \rangle} \quad (113)$$

where E is the energy (kinetic plus potential) of the wave per unit area of the interface, and the brackets mean averaging over x ,

$$\begin{aligned} \langle E \rangle &= \left\langle \int \rho v_z^2 dz \right\rangle = \rho \left\langle \int \left(\frac{\partial \Phi}{\partial z} \right)^2 dz \right\rangle = 2\rho k^2 \int \langle \Phi^2 \rangle dz \\ \left\langle \frac{dE}{dt} \right\rangle &= -2\eta \left\langle \int \left(\frac{\partial v_z}{\partial x} \right)^2 dz \right\rangle = -2\eta \left\langle \int \left(\frac{\partial^2 \Phi}{\partial x \partial z} \right) dz \right\rangle \\ &= -8\eta k^2 \int \langle \Phi^2 \rangle dz \end{aligned} \quad (114)$$

This gives,

$$\varepsilon = \frac{2\eta k^2}{\rho} = \frac{2\eta \omega^{4/3}}{\rho^{1/3} \gamma^{2/3}} \quad (115)$$

Since the addition of surfactant causes a decrease in the surface tension, it will enhance the damping of capillary waves.

The second limiting case is where the adsorbed film is considered incompressible. Such a film will significantly confine the motion the liquid as the no-slip condition holds at the boundary between the film and the liquid. Real films also have a finite value of the bending modulus, but the bending energy can be neglected as long as the amplitude of waves is much less than the wavelength. Assuming further that $\eta \ll \rho \lambda^2 \omega$, one can approximate the velocity field near the liquid/vapour interface by $\mathbf{v}=(v_x, 0, 0)$ where

$$v_x = v_0 \exp(-i\omega t) \left\{ 1 - \exp \left[(i-1)z \left(\frac{\rho \omega}{2\eta} \right)^{1/2} \right] \right\} \quad (116)$$

The stress experienced by the film due the liquid motion is

$$f_x = \eta \frac{\partial v_x}{\partial z} \Big|_{z=0} = \left(\frac{\rho \omega \eta}{2} \right)^{1/2} (i-1) v_x \Big|_{z=0} \quad (117)$$

and correspondingly, the average energy dissipation per unit area per unit time can be estimated as

$$\langle dE/dt \rangle = -\langle f_x v_x \rangle \alpha - v_0^2 (\rho \omega \eta)^{1/2} \quad (118)$$

whereas the total energy of the wave is

$$\langle E \rangle = \rho \left\langle \int v_x^2 dz \right\rangle \alpha \rho v_0^2 \left(\frac{\eta}{\rho \omega} \right)^{1/2} = v_0^2 \left(\frac{\rho \eta}{\omega} \right)^{1/2} \quad (119)$$

Hence, the damping coefficient in the latter case scales as

$$\varepsilon \propto \frac{\omega^{7/6} \eta^{1/2}}{\gamma^{1/3} \rho^{1/6}} \quad (120)$$

and can be much greater than that calculated by Eq. (115) in the case of sufficiently long waves. This explains why dense adsorbed surfactant films strongly influence the dynamics of capillary waves.

8. Concluding remarks

Understanding the underlying physical factors controlling the interfacial behaviour of surfactant molecules has been of interest to surface scientists for several decades now. From the experimental viewpoint, the most challenging aspect of this work has always been the ability to distinguish a thin surface layer from the overwhelming bulk substance. Over the past two decades, a substantial progress in understanding the microstructure of surfactants at interfaces has been achieved by using neutron reflection and atomic force microscopy, which significantly strengthen the scientific arsenal of the researchers working in this field. Not only did it become possible to visualize the surface structures but also to study their internal organisation and response to external disturbances. The gathered knowledge brings to life new insights into the dynamic properties of interfaces in relation to surface rheology and supramolecular organization at functionalized surfaces. Neutron and X-ray scattering methods allow one to go down the nanometer and picosecond resolutions in studying the structure and dynamics of aggregated surfactants. Novel spectroscopic techniques such as external-reflection Fourier transform infrared spectroscopy (ERFTIR) and vibrational sum frequency spectroscopy (VSFS) have the potential to measure quantitatively the surface coverage and composition in pure and mixed monolayers. The inherent surface sensitivity of VSFS makes it an advantageous method of studying the molecules at interfaces. Some hybrid techniques such as spectroscopic ellipsometry also are coming into use. Recent theoretical developments concern the depletion and surface-induced structural forces in thin micellar films, surface tension relaxation in micellar solutions, the mechanism of super-spreading, phase transitions in lipid monolayers at the air/water interface, etc. Much less progress has been made in understanding surface interactions on a molecular level, especially when solid surfaces in contact with another condensed phase are concerned.

References

- [1] Azzam RMA, Bashara NM. *Ellipsometry and polarized light*. Amsterdam: North-Holland; 1977.
- [2] Clint JH. *Surfactant aggregation*. Glasgow: Blackie; 1992.
- [3] Mizusaki M, Morishima Y. *J Phys Chem, B* 1998;102:1908.
- [4] D'Alagni M, D'Archivio AA, Galantini L, Giglio E. *Langmuir* 1997;13:5811.
- [5] Soderman O, Herrington KL, Kaler EW, Miller DD. *Langmuir* 1997;13:5531.
- [6] Swanson-Vethamuthu M, Dubin PL, Almgren M, Li Y. *J Colloid Interface Sci* 1997;186:414.
- [7] Zhang H, Dubin PL. *J Colloid Interface Sci* 1997;186:264.
- [8] Guenoun P, Lipsky S, Mays JW, Tirrell M. *Langmuir* 1996;12:1425.
- [9] Zana R. *Langmuir* 1996;12:1208.
- [10] Griffiths PC, Cheung AYF, Finney GJ, Farley C, Pitt AR, Howe AM, et al. *Langmuir* 2002;18:1065.
- [11] Hansson P, Almgren M. *J Phys Chem* 1995;99:16684.
- [12] Quina FH, Nassar PM, Bonilha JBS, Bales BL. *J Phys Chem* 1995;99:17028.
- [13] Imae T, Hayashi N. *Langmuir* 1993;9:3385.
- [14] Thomas RK, Penfold J. *J Phys, Condens Matter* 1990;2:1369.
- [15] Corn RM, Higgins DA. *Chem Rev* 1994;94:107.
- [16] Mawie S, Cleveland JP, Gaub HE, Stucky GD, Hausma DK. *Langmuir* 1994;10:4409.
- [17] Davies JT, Rideal EK. *Interfacial phenomena*. 2nd ed. New York: Academic Press; 1963.
- [18] Fainerman VB, Aksenenko EV, Miller R. *J Phys Chem, B* 2000;104:5744.
- [19] Franses EI, Siddiqui FA, Ahn DJ, Chang C-H, Wang N-HL. *Langmuir* 1995;11:3177.
- [20] Aratono M, Villeneuve M, Takiue T, Ikeda N, Iyota H. *J Colloid Interface Sci* 1998;200:161.
- [21] Fainerman VB, Miller R, Möhwald H. *J Phys Chem, B* 2002;106:809.
- [22] Fainerman VB, Miller R, Aksenenko EV. *Langmuir* 2000;16:4196.
- [23] Kralchevsky PA, Danov KD, Broze G, Mehreteab A. *Langmuir* 1999;15:2351.
- [24] Zhmud B, Bergström L. In: Schwarz JA, Contescu C, editors. *Surface of nanoparticles and porous materials*. New York: Marcel Dekker; 1999 [chap. 21].
- [25] Adamson AW. *Physical chemistry of surfaces*. 5th ed. New York: John Wiley; 1990.
- [26] Padday JF. In: Matijević E, editor. *Surface and colloid science*, vol. 1. New York: Wiley-Interscience; 1969. p. 101.
- [27] MacLeod CA, Radke CJ. *J Colloid Interface Sci* 1993;160:452.
- [28] MacLeod CA, Radke CJ. *J Colloid Interface Sci* 1994;166:73.
- [29] Defay R, Pètré G. In: Matijević E, editor. *Surface and colloid science*, vol. 3. New York: Wiley-Interscience; 1971. p. 27.
- [30] Born M, Wolf E. *Principles of optics*. 4th ed. Oxford: Pergamon Press; 1968.
- [31] Frantz P, Granick S. *Phys Rev Lett* 1992;66:899.
- [32] Tiberg F. *J Chem Soc, Faraday Trans* 1996;92:531.
- [33] Tiberg F, Jönsson B, Lindman B. *Langmuir* 1994;10:3714.
- [34] Brinck J, Tiberg F. *Langmuir* 1996;12:5042.
- [35] Tiberg F, Jönsson B, Tang J-A, Lindman B. *Langmuir* 1994;10:2294.
- [36] Tiberg F, Landgren M. *Langmuir* 1993;9:927.
- [37] Russel WB, Saville DA, Schowalter WR. *Colloidal dispersions*. Cambridge University Press; 1989.
- [38] Higgins JS, Stein RS. *J Appl Crystallogr* 1978;11:346.
- [39] Feigin LA, Svergun DI. In: Taylor GW, editor. *Structure analysis by small-angle X-ray and neutron scattering*. New York: Plenum Press; 1987.
- [40] Willis BJM. *Chemical applications of neutron scattering*. Oxford: Oxford University Press; 1973.
- [41] Ottewill RH. In: Goodwin JW, editor. *Colloidal dispersions*. Special Publication, vol. 43. Royal Society of Chemistry.
- [42] Higgins JS, Benoit HC. *Polymers and neutron scattering*. Oxford series on neutron scattering in condensed matter, vol. 8. Clarendon Press; 1994.
- [43] Sears VF. *Neutron news* 1992;3:26.
- [44] Schmitz KS. *An introduction to dynamic light scattering by macromolecules*. Boston: Academic Press; 1990.
- [45] Penfold J, Staples EJ, Thompson L, Tucker I, Hines J, Thomas RK, et al. *Langmuir* 1995;11:2496.
- [46] He L, Garamus VM, Funari SS, Malfois M, Willumeit R, Niemeyer B. *J Phys Chem, B* 2002;106:7596.
- [47] Chen SH. *Annu Rev Phys Chem* 1986;37:351.
- [48] Chevalier Y, Zemb T. *Rep Prog Phys* 1990;53:279.
- [49] Pynn R. *Neutron scattering: a primer*. Los Alamos Neutron Science Center; 1990.
- [50] Penfold J, Staples EJ, Tucker I, Thompson LJ, Thomas RK. *Physica B* 1998;248:223.
- [51] Sinha SK. *Physica B* 1991;173:25.

- [52] Penfold J. *Physica B* 1991;173:1.
- [53] Lu JR, Thomas RK, Penfold J. *Adv Colloid Interface Sci* 2000;84:143.
- [54] Delmon B. *Introduction a la Cinétique Hétérogène*. Paris: Editions Technip; 1969.
- [55] Joos P. *Dynamic surface phenomena*. Utrecht, The Netherlands: VSP; 1999.
- [56] Zhmud B, Tiberg F, Kizling J. *Langmuir* 2000;16:7685.
- [57] Zhmud BV, Tiberg F, Kizing J. *Langmuir* 2000;16:2557.
- [58] Fainerman VB, Rakita YuM, Zadara VM. *Zh Fiz Khim* 1984;58:2006.
- [59] Filippov LK, Filippova NL. *J Colloid Interface Sci* 1997;187:304.
- [60] Dushkin CD. *Colloids Surf, A Physicochem Eng Asp* 1998;143:283.
- [61] Ariel G, Diamant H, Andelman D. *Langmuir* 1999;15:3574.
- [62] Holland PM. In: Holland PM, Rubingh DN, editors. *Mixed surfactant systems*. Washington: ACS; 1992. p. 31.
- [63] Goloub TP, Pugh RJ, Zhmud B. *J Colloid Interface Sci* 2000;229:72.
- [64] Rubingh DN. *Solution chemistry of surfactants*. New York: Plenum Press; 1979.
- [65] Lin S-Y, Tsay R-Y, Lin L-W, Chen S-I. *Langmuir* 1996;12:6530.
- [66] Lin S-Y, McKeigue K, Maldarelli C. *Langmuir* 1991;7:1055.
- [67] Nikas YJ, Puvvada S, Blankschtein D. *Langmuir* 1992;8:2680.
- [68] Eastoe J, Paul A, Rankin A, Wat R. *Langmuir* 2001;17:7873.
- [69] Dupont A, Eastoe J, Barthélémy P, Pucci B, Heenan R, Penfold J, et al. *J Colloid Interface Sci* 2003;261:184.
- [70] Bell GR, Manning-Benson S, Bain CD. *J Phys Chem, B* 1998;102:218.
- [71] Lee EM, Thomas RK, Penfold J, Ward RC. *J Phys Chem* 1989;93:381.
- [72] Simister EA, Lee EM, Thomas RK, Penfold J. *J Phys Chem* 1992;96:1373.
- [73] Lu JR, Li ZX, Thomas RK, Penfold J. *J Chem Soc, Faraday Trans* 1996;92:403.
- [74] McDermott DC, McCarny J, Thomas RK, Rennie AR. *J Colloid Interface Sci* 1994;162:304.
- [75] Atkin R, Craig VSJ, Biggs S. *Langmuir* 2001;17:6155.
- [76] Atkin R, Craig VSJ, Wanless EJ, Biggs S. *J Phys Chem, B* 2003;107:2978.
- [77] Lu JR, Lee EM, Thomas RK, Penfold J, Flitsch S. *Langmuir* 1993;9:1352.
- [78] Lu JR, Li ZX, Thomas RK, Staples EJ, Thompson L, Tucker I, et al. *J Phys Chem* 1994;98:6559.
- [79] Campbell RA, Bain CD. *Vibr Spectrosc* 2004;35:205.
- [80] Richmond GL. *Chem Rev* 2002;102:2693.
- [81] Shen YR. *Nature* 1989;337:519.
- [82] Bloembergen N, Simmon HJ, Lee CH. *Phys Rev* 1969;181:1261.
- [83] Lu JR, Marrocco A, Su TJ, Thomas RK, Penfold J. *J Colloid Interface Sci* 1993;158:303.
- [84] Hassan PA, Fritz G, Kaler EW. *J Colloid Interface Sci* 2003;257:154.
- [85] Belaroui F, Cabane B, Dorget M, Grohens Y, Marie P, Holl Y. *J Colloid Interface Sci* 2003;262:409.
- [86] Almgren M, Gimel JC, Wang Ke, Karlsson G, Edwards K, Brown W, et al. *J Colloid Interface Sci* 1998;202:222.
- [87] Staples E, Penfold J, Tucker I. *J Phys Chem, B* 2000;104:606.
- [88] Tiberg F, Brinck J, Grant L. *Curr Opin Colloid Interface Sci* 2000;4:411.
- [89] Manne S, Cleveland JP, Gaub HE, Stucky GD, Hansma PK. *Langmuir* 1994;10:4409.
- [90] Manne S, Gaub HE. *Science* 1995;270:1480.
- [91] Grant LM, Tiberg F, Ducker WA. *J Phys Chem, B* 1998;102:4288.
- [92] Holand NB, Ruegsegger M, Marchant RE. *Langmuir* 1998;14:2790.
- [93] Ducker WA, Wanless EJ. *Langmuir* 1999;15:160.
- [94] Atkin R, Craig VSJ, Wanless EJ, Biggs S. *Adv Colloid Interface Sci* 2003;103:219.
- [95] Grant L, Ederth T, Tiberg F. *Langmuir* 2000;16:2285.
- [96] Spicer PT, Hayden KL, Lynch ML, Ofori-Boateng A, Burns JL. *Langmuir* 2001;17:5748.
- [97] Montalvo G, Valiente M, Rodenas E. *J Colloid Interface Sci* 1995;172:494.
- [98] Danino D, Talmon Y, Zana R. *J Colloid Interface Sci* 1997;186:170.
- [99] Gustafsson J, Nylander T, Almgren M, Ljusberg-Wahren H. *J Colloid Interface Sci* 1999;211:326.
- [100] Li X, Kunieda H. *J Colloid Interface Sci* 2000;231:143.
- [101] Nakano M, Sugita A, Matsuoka H, Handa T. *Langmuir* 2001;17:3917.
- [102] von Bahr M, Tiberg F, Zhmud B. *Langmuir* 1999;15:7069.
- [103] Teletzke GF, Davis HT, Scriven LE. *Chem Eng Commun* 1987;55:41.
- [104] Eggleton CD, Pawar YP, Stebe KJ. *J Fluid Mech* 1999;385:79.
- [105] Rafai S, Sarker D, Bergeron V, Meunier J, Bonn D. *Langmuir* 2002;18:10486.
- [106] Nikolov AD, Wasan DT, Chengara A, Koczo K, Policello G, Kolossvary I. *Adv Colloid Interface Sci* 2002;96:325.
- [107] Battal T, Bain CD, Weiß M, Darton RC. *J Colloid Interface Sci* 2003;263:250.
- [108] Shen AQ, Gleason B. *Phys Fluids* 2002;14:4055.
- [109] Landau LD, Lifshitz EM. *Hydrodynamics*. 3d ed. Moscow: Nauka; 1986.